University of Alberta

Fatigue Performance of Long-fiber-reinforced Polymers (FRPs) in Relation with Matrix Properties

By

Yemi Setiadi

A thesis submitted to the Faculty of Graduate Studies and Research in partial fulfillment of the requirements for the degree of *Master of Science*

Department of Mechanical Engineering

Edmonton, Alberta

Spring 2005

0-494-08147-3

Library and Archives Canada

Published Heritage Branch

395 Wellington Street
Ottawa ON K1A 0N4
Canada

Bibliothèque et Archives Canada

Direction du Patrimoine de l'édition

395, rue Wellington
Ottawa ON K1A 0N4
Canada

Your file *Votre référence*
ISBN:
Our file *Notre reference*
ISBN:

NOTICE:
The author has granted a non-exclusive license allowing Library and Archives Canada to reproduce, publish, archive, preserve, conserve, communicate to the public by telecommunication or on the Internet, loan, distribute and sell theses worldwide, for commercial or non-commercial purposes, in microform, paper, electronic and/or any other formats.

The author retains copyright ownership and moral rights in this thesis. Neither the thesis nor substantial extracts from it may be printed or otherwise reproduced without the author's permission.

AVIS:
L'auteur a accordé une licence non exclusive permettant à la Bibliothèque et Archives Canada de reproduire, publier, archiver, sauvegarder, conserver, transmettre au public par télécommunication ou par l'Internet, prêter, distribuer et vendre des thèses partout dans le monde, à des fins commerciales ou autres, sur support microforme, papier, électronique et/ou autres formats.

L'auteur conserve la propriété du droit d'auteur et des droits moraux qui protège cette thèse. Ni la thèse ni des extraits substantiels de celle-ci ne doivent être imprimés ou autrement reproduits sans son autorisation.

In compliance with the Canadian Privacy Act some supporting forms may have been removed from this thesis.

While these forms may be included in the document page count, their removal does not represent any loss of content from the thesis.

Conformément à la loi canadienne sur la protection de la vie privée, quelques formulaires secondaires ont été enlevés de cette thèse.

Bien que ces formulaires aient inclus dans la pagination, il n'y aura aucun contenu manquant.

Canada

Abstract

Better mechanical properties and fatigue performance of engineering materials are always desired in structural applications. In this study, in-plane random glass fiber which is a relatively new reinforcement in fiber-reinforced polymers (FRPs) was embedded in polymers (i.e. polyester and polyurethane). Mechanical properties of the polymers and FRPs were determined from static tests. Zero-tension fatigue loading of FRPs was conducted in order to study damage development, modulus degradation, and energy dissipation rate.

It was concluded that polyurethane-based FRP showed better fatigue resistance than polyester-based FRP at the applied load of 50% of their respective ultimate tensile strength (UTS), as indicated by longer fatigue lifetime, milder modulus degradation, and higher energy dissipation rate. Modulus degradation and energy dissipation rate were found to be correlated to damage development. The resistance to crack propagation in the polyurethane-based FRP was found to be related to the higher fracture toughness of the matrix.

Acknowledgements

I am particularly indebted to my supervisors, Dr. P. -Y. Ben Jar and Dr. J. -J. R. Cheng for their guidance and financial support throughout this study. Also, I am grateful to Dr. T. Kuboki for his invaluable experimental supervision and discussions.

I would like to thank Mr. Bernie Faulker, Mrs. Tuula Hilvo, Mr. Dave Pape, and Mr. Albert Yuen who offered me the excellent technical help and precious discussions.

Special thanks go out to ISIS, Canada and Natural Science and Engineering Research Council of Canada (NSERC) for the financial support throughout the study.

My appreciation goes to the members of the Durable Materials Research Lab: Mr. Chengye Fan, Mr. Lei Ji, Mr. Hyock-Ju Kwon, Mr. Emran Rashed, Mr. Tadayoshi Yamanaka for their friendship and provision of a pleasant environment.

Finally, my gratitude must be given to my parents, Andrias and Go Swan Hwa and my sisters, Heli Eunike and Heidy Christina for their support throughout the study.

TABLE OF CONTENTS

1. Introduction 1

1.1 Scope of the Study 3

1.2 Literature Review 5

2. Materials Information and Fabrication 10

2.1 Molds 13

2.1.1 Mold Type 1 13
2.1.2 Mold Type 2 14
2.1.3 Mold Type 3 14

2.2 Polyester Resin Casts and Polyester-based FRP 15

2.2.1 Resin Casts for Tensile and Fracture Toughness Tests 15
2.2.2 Polyester-based FRP for Tensile and Fatigue Tests 16

2.3 Polyurethane Resin Casts and Polyurethane-based FRP 17

2.3.1 Resin Casts for Tensile and Fracture Toughness Tests 17
2.3.2 Polyurethane-based FRP for Tensile and Fatigue Tests 18

2.4 Fiber Volume Fraction and Void Content Calculation 20

2.4.1 Fiber Volume Fraction 20
2.4.2 Void Content of Resin Casts 23
2.4.3 Void Content of FRPs 24

3. Specimens Preparation and Test Methodology 28

3.1 Tensile Test 28

3.2 Fatigue Test 29

3.3 Plain-strain Fracture Toughness Test 33

4. Results and Discussions 36

4.1 Tensile Test 36

4.1.1 Resin Casts 36
4.1.2 Fiber-reinforced Polymers (FRPs) 39
4.1.3 Macroscopic and Microscopic Observations 42

4.2 Fatigue Test 45

4.2.1 Mechanical Properties under Fatigue Loading 45
4.2.2 Macroscopic and Microscopic Observations 64

4.3 Plain-strain Fracture Toughness Tests 75

4.4 Synthesis of the Fatigue Behaviour 77

5. Conclusions and Recommendations for the Future Studies 80

6. Bibliography 83

LIST OF FIGURES

Figure 1.1. Modulus degradation in sheet molding compound (Wang and Chim [13]). 7

Figure 1.2. Crack profile in graphite/polycarbonate (Mandell et al. [38]). 8

Figure 2.1. Randomly oriented fiber mat used in this study. 11

Figure 2.2. Mold type 1 13

Figure 2.3. Mold type 2 14

Figure 2.4. Mold type 3 15

Figure 2.5. FRP panels: (a) polyester-based FRP and polyurethane-based FRP type 1 and (b) polyurethane-based FRP type 2 20

Figure 2.6. Sizing mass versus pure fiber mass. 25

Figure 3.1. MTS model 812 material testing machine 29

Figure 3.2. Geometry and dimensions of the specimens for tensile and fatigue tests. 30

Figure 3.3. MTS model 810 material testing machine 30

Figure 3.4. Cyclic loading function of the fatigue test. 31

Figure 3.5. Load-displacement response under cyclic loading of the FRPs. 32

Figure 3.6. 220 kN Instron machine. 34

Figure 3.7. Geometry and dimensions of the specimens for fracture toughness test 35

Figure 4.1. SEM micrograph of fracture surface of pure polyurethane after tensile test. 37

Figure 4.2. Stress-strain response of resin casts. 38

Figure 4.3. Stress-strain response of FRPs. 42

Figure 4.4. Images of tensile-fractured specimens: (a) polyester-based FRP, (b) polyurethane-based FRP type 1, and (c) polyurethane-based FRP type 2 43

Figure 4.5. Micrographs viewed in Y-direction (referred to Figure 3.2) for tensile-fractured specimens near the fracture surface: (a) polyester-based FRP, (b) polyurethane-based FRP type 1, and (c) polyurethane-based FRP type 2..... 45

Figure 4.6. Linear plots of cumulative strains versus number of cycles: (a) polyester-based FRP, (b) polyurethane-based FRP type 1, (c) polyurethane-based FRP type 2 at 0-95.2 MPa, and (d) polyurethane-based FRP type 2 at 0-87.6 MPa. 50

Figure 4.7. Semi-logarithmic plots of absolute modulus versus number of cycles: (a) polyester-based FRP, (b) polyurethane-based FRP type 1, (c) polyurethane-based FRP type 2 at 0-95.2 MPa, and (d) polyurethane-based FRP type 2 at 0-87.6 MPa. 54

Figure 4.8. Semi-logarithmic plots of normalized modulus versus number of cycles: (a) polyester-based FRP, (b) polyurethane-based FRP type 1, (c) polyurethane-based FRP type 2 at 0-95.2 MPa, and (d) polyurethane-based FRP type 2 at 0-87.6 MPa. 57

Figure 4.9. Typical plots of normalized modulus versus number of cycles of FRPs: (a) semi-logarithmic plot and (b) linear plot. 59

Figure 4.10. Semi-logarithmic plots of energy dissipation rate versus number of cycles: (a) polyester-based FRP, (b) polyurethane-based FRP type 1, (c) polyurethane-based FRP type 2 at 0-95.2 MPa, and (d) polyurethane-based FRP type 2 at 0-87.6 MPa. 62

Figure 4.11. A typical semi-logarithmic plot of energy dissipation rate versus number of cycles of FRPs 63

Figure 4.12. Photographs of virgin (left-hand side) and fatigue-fractured FRPs (right-hand side). 65

Figure 4.13. Micrographs viewed in Y-direction (referred to Figure 3.2) of polyester-based FRP: (a) 1,000 cycles, where the matrix cracking was about to develop and (b) 52,897 cycles (fracture). 67

Figure 4.14. Micrographs viewed in Y-direction (referred to Figure 3.2) of polyurethane-based FRP type 1: (a) 1,000 cycles, where no matrix cracking was developed, (b) 10,000 cycles, where matrix cracking was about to develop, and (c) 40,000 cycles, where matrix cracking had been developed..... 70

Figure 4.15. Micrographs viewed in Y-direction (referred to Figure 3.2) of polyurethane-based FRP type 2 at 0-95.2 MPa: (a) 1,000 cycles, where no matrix cracking was developed, (b) 10,000 cycles, where matrix cracking was about to

develop, and (c) 39,001 cycles (fracture), where matrix cracking had been developed. 72

Figure 4.16. Micrographs viewed in Y-direction (referred to Figure 3.2) of polyurethane-based FRP type 2 at 0-87.6 MPa: (a) 1,000 cycles, where few interfacial cracks were observed, (b) 10,000 cycles, where many interfacial cracks were observed, (c) 40,000 cycles, where matrix cracking was about to develop, and (d) 69,882 cycles (fracture), where matrix cracking had been developed. 74

1. Introduction

Since early civilizations, man has combined materials together in the form of laminates, dispersed particles or fibers into a continuous material, for example bricks, furnaces, etc. [1,2]. These materials are now called composites. A composite is a material which consists of two of more constituents with distinct materials interface separating the components. The constituents are combined at a macroscopic level and are not soluble in each other. One constituent is called the reinforcing phase, and the one in which it is embedded is called the matrix. The reinforcing material may be in the form of fibers, particles, or flakes. The matrix phases are generally continuous. By doing so, it was possible to obtain combinations of strength or toughness with other properties that could not be found with any single component alone. Although these ancient materials can be broadly classified as a type of composite materials, the modern science of composite materials began recently.

As modern technology has developed, so has the interest in composites, many of which include fiber as one of the reinforcements and a polymer as one of the matrix constituents [3]. Fiber-reinforced polymers (FRPs) are increasingly used in the aerospace and other structural applications because of their combination of high specific stiffness (stiffness to density ratio) and high specific strength (strength to density ratio) and potentially low unit cost through the ability to manufacture large complex components in single operations with minimal material wastage. Other benefits are good corrosion resistance and fatigue behaviour [4].

Apart from technological importance, composites are also of fundamental concern in material science. While their properties are frequently defined by some average of constituent properties, interactive effects of the reinforcement and matrix are frequently present. Thus, characterization of composite behaviour is complicated in interesting ways by the fact that a nominally two-component system contains interfaces and discrete interfacial regions are often difficult to infer, especially under fatigue loading [3]. Fatigue itself is failure of a component by the repeated application of a varying load of which maximum amplitude below its ultimate tensile strength. All materials, except very brittle material such as glasses, are susceptible to fatigue [5]. Almost all engineering components are subjected to varying loads throughout their working life, and fatigue is easily the most common and least understood cause of failure.

Fatigue failure in FRPs generally involves several damage mechanisms that are combined in leading to final fracture. From the microstructural point of view, FRPs are heterogeneous materials that have inherently various kinds of microscopic stress concentrators such as fiber ends, fiber/matrix interfaces, voids, etc. However, stress concentration is not the only factor that affects their fatigue behaviour. Other factors such as specimen geometry, type of fiber reinforcement, matrix properties, interfacial bonding, environment, temperature, stress level, etc. also influence the fatigue behaviour significantly. Additional complications include (1) viscoelastic nature of the polymer matrix, (2) widely variable criteria for failure, and (3) complex nature of damage development [3]. Hence, understanding the roles of these factors on fatigue behaviour of FRPs is essential for assigning an appropriate loading level to structures that are concerned with fatigue strength.

It is not an easy task to develop an analytical model that can cover all parameters presented above because of the interaction of failure mechanisms. Therefore, experimental work is conducted in order to give a better understanding. Laboratory tests show a wide statistical scatter in fatigue; translating their results into design data is not an easy task, and will not be attempted here. Thus, fundamental understanding of the fatigue behaviour of polymeric composites poses a strong challenge to the scientists.

1.1 Scope of the Study

FRPs investigated in this study were those fabricated using the same reinforcement (continuous glass fiber with random in-plane orientation), but different thermosetting resins, either polyester or polyurethane. This type of FRPs is extensively used in many structural and load-bearing applications because they have relatively isotropic properties in the reinforced plane and can be molded into complex shapes when compared to conventional FRP with aligned fiber reinforcement. Thermosetting resins are commonly used for composites subjected to the most severe conditions because of their higher modulus and dimensional stability, especially at elevated temperature [3].

It was known that the use of higher performance carbon fiber gave little improvement in either tensile properties or fatigue lifetime of FRP that had standard epoxy resin as the matrix [6]. Talreja [7] and Van Der Oever [8] have shown that for glass fiber composites, cracks in the matrix and at the fiber/matrix interface would be the predominant damage mechanisms when loading is in directions off the fiber reinforcement. In general, fatigue behaviour of FRP is known to be mainly dominated by

interfacial bonding between fiber and matrix and matrix properties such as those for yielding, plastic flow, cracking, and other non-linear matrix deformation [9]. Therefore, matrix of FRP plays an important role in damage initiation and propagation under fatigue loading because of its primary influence in carrying transverse and shear loading.

Several techniques have been developed to predict FRPs' fatigue behaviour, especially the reduction of mechanical properties with the increase of the number of loading cycles [10-13]. The most common model, known as wear-out model, is particularly concerned with reduction in strength and modulus with fatigue loading. The model uses the change in these properties as an indicator of the extent of fatigue damage development [12-18]. Several indicators of damage development have been considered, among which the energy-based parameters were found to be very effective. For example, energy dissipation rate served well to characterize the irreversible nature of the damage that was caused by cyclic loading [19-21].

In this study, mechanical properties of the polymers and FRPs will be presented from static tests. Fatigue tests were only conducted on FRPs and the results will be discussed. Modulus degradation and energy dissipation rate under fatigue loading and the corresponding damage development process were investigated for polyester-based FRP with no void observed and polyurethane-based FRP with void content of 4.8% (type 1) and 2.6% (type 2). The cyclic loading level was from 0 to 50% of their ultimate tensile strength (UTS) and an additional fatigue test was conducted on polyurethane-based FRP type 2 at the same absolute stress level as polyurethane-based FRP type 1 to study the effect of void content. Variation of mechanical properties during the fatigue loading, including number of cycles to fracture, modulus degradation, energy dissipation rate, and

their relationship with damage development process are discussed. The particular focus of the current study is the role of matrix toughness, interfacial bonding, and effect of void content on fatigue resistance of the polyurethane-based FRP.

1.2 Literature Review

There has been over 40 years of analytical and experimental investigation of composite structures under fatigue loading. However, reports on the damage evolution and property degradation in the random fiber-reinforced polymers have been limited because of the late entry of this class of materials and complex nature of damage development under fatigue loading. This literature review is intended to point out the major trend of the experimental results through selective references, but not to cover all work published in the past.

Smith and Owen [10] examined fatigue properties of chopped strand mat (CSM) FRP based on polyesters of low- and high-reactivity. They found that variation of fiber content over a range of 29 to 36% by weight had a considerable effect on the tensile strength, but only a small or almost negligible effect on fatigue strength. In addition, the results showed no noticeable difference between FRPs with low- and high-reactivity resins as the matrix. Later on they suggested [14] that internal damage in laminates, initiated by debonding between fiber and matrix, could be detected by means of loss in modulus. Using the loss in modulus as a damage indicator, they found that the two resins of different reactivity had negligible difference in bonding strength with fiber, but the

low-reactivity resin had higher matrix resistance to crack development. It was suggested that the high resistance to crack development was due to its greater strain to failure.

Owen and Rose [16] investigated the effects of ductility of polyester resin on mechanical properties and damage mechanisms of FRP under tensile and fatigue loading. The matrix was modified by adding 0 to 50% by weight of a ductile resin to a base resin, to yield a wide range of FRP with different matrix ductility. The reinforcements used were CSM with fiber length around 50 mm and satin-weave fabric. The specimens for tensile test conformed to ASTM D 638-64T. For fatigue test, a dumb-bell specimen with circular arc profile was used. It was found that the ultimate tensile strength of both resin casts and laminates showed a maximum with the content of ductile resin in the range between 10 and 15%. However, the tensile modulus decreased steadily with the increase of the content of the ductile resin. Strain to failure was found to increase with the ductile resin content to the limit of 20% of the ductile resin for both laminates and resin casts, and then remained essentially constant for the laminates, but increased rapidly for the resin casts. The addition of ductile resin was found to delay the onset of debonding and matrix cracking in fatigue tests. However, such an effect did not cause any significant difference in fatigue lifetime under zero-tension loading when the number of cycles for fracture was in the range of 10^3 to 10^6.

Soldatos et al. [22] reported that high elongation is not the only prerequisite to increasing FRPs strength under flexural fatigue loading; resin must also have high tensile strength i.e. high toughness (area under stress-strain curve) of FRPs. A study of tension-tension fatigue loading, but using unidirectional carbon-fiber-reinforced polymers, was reported by Gamstedt and Talreja [23]. They found that even with a tougher matrix, poly-

ether-ether-ketone (PEEK), the fatigue resistance was not improved, as compared to epoxy. It was concluded that a tougher matrix did not necessarily provide a better fatigue performance to the FRP. Suppression of the progressive debonding and the matrix cracking is the key factor to improve the fatigue resistance.

Another study of damage development and property degradation of FRP by fatigue loading was reported by Wang and Chim [13]. The fiber reinforcement and resin used were roving-glass chopped to a length of 25.4 mm and polyester, respectively. The cyclic loading, at a level ranging from 20% to 85% of the ultimate tensile strength of the FRP, was applied at a frequency of 2 Hz. It was found that the modulus showed a different trend by varying the loading levels. When subjected to 85% of the ultimate tensile strength, the modulus dropped rapidly, compared to that at 20% of the ultimate tensile strength as shown in Figure 1.1. A damage parameter was proposed to describe quantitatively the degree of homogeneity of the fatigue damage by assuming the crack density (cracks per unit area) may be averaged throughout the bulk of material as being uniform and homogenous in continuum sense. This may be used in a stiffness-based fatigue failure criterion.

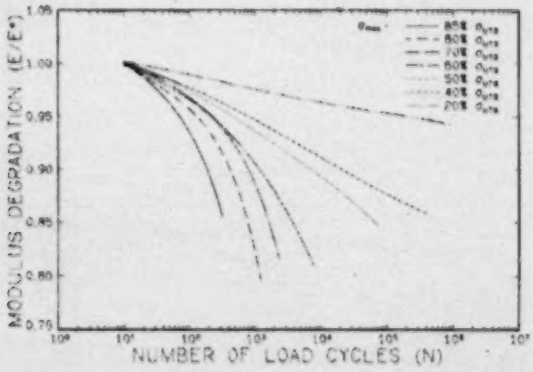

Figure 1.1. Modulus degradation in sheet molding compound (Wang and Chim [13]).

Studies on fracture toughness based on linear elastic fracture mechanics (LEFM) of FRPs have been reported by many researchers [24-38]. Most studies have been conducted on short fiber reinforcements. Difficulty has been reported in many studies in obtaining crack growth in the desired direction, as cracks tended to deviate to be parallel to the dominant fiber orientation [35]. The fiber orientation must be chosen carefully so that proper tests can be run. Toughness can be considerably lower if the crack grows parallel to the primary fiber direction. The crack was found to be a single crack macroscopically [39], but followed a zigzag fiber avoidance growth pattern around major fibers, as shown in Figure 1.2.

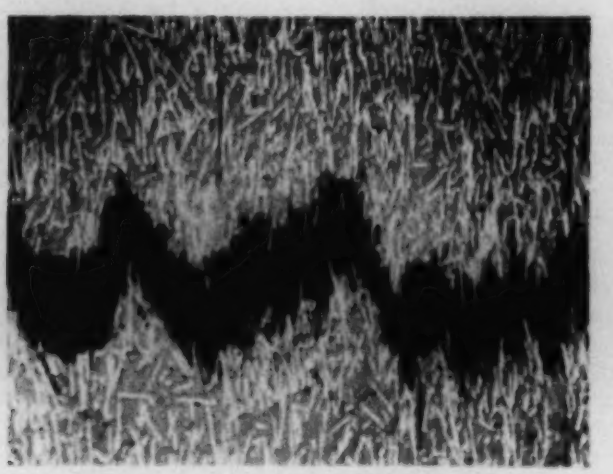

Figure 1.2. Crack profile in graphite/polycarbonate (Mandell et al. [38]).

Owen et al. [29] conducted fracture toughness test on short fiber reinforced polyester. They found that the values of critical stress intensity factor, K_C, were relatively independent of the crack length in the specimen. Independency of crack length on fracture toughness of FRPs was also observed by Mandell et al. [35] and Wang et al.

[37]. Interestingly, several researchers [38,40-42] have reported their experiment findings on fatigue crack propagation in short fiber-reinforced polymers that generally followed the Paris crack propagation law (i.e. $da/dN = C(\Delta K)^m$). They found linear relationships between log da/dN and log ΔK. The exponent, m, was found to be approximately double for the FRPs, as compared to unreinforced polymers [38].

Fracture toughness measurements in composites are still questionable due to limitations of the theory. The theoretical justification for this relation is based on the analysis of the continuous extension of a crack in isotropic and homogeneous materials. Another limitation is that plastic zone in front of crack tip must be small. In FRPs, stress-strain distribution in front of crack tip is difficult to infer and not uniformly distributed because the reinforcement that exists in the matrix acts as a crack arrester. Many modes of failure, for example debonding, fiber fracture, and fiber pull-out are radically different from those assumed in the Griffith-Irwin-Orowon approach [43,44]. Due to the unanswered questions above, no standard test method for measuring fracture toughness in FRP is established yet. Hence, fracture toughness tests on FRPs were not attempted here in the study.

2. Materials Information and Fabrication

Glass fibers are the most common fiber used in FRPs. Nowadays glass fibers account for an estimated 95% of the total fiber consumption for polymer reinforcement [45]. The advantages of glass fibers are excellent performance/cost ratio, high thermal resistance, good insulating properties, and low coefficient of thermal expansion. However, the drawbacks include low elastic modulus, poor adhesion to polymers, high specific gravity, sensitive to abrasion (reduces tensile strength), and low fatigue strength [46].

The reinforcement selected in this study was continuous E-glass fiber that was randomly oriented and supplied in a form of fiber mat of 1.5 oz/yard^2, as shown in Figure 2.1. The glass fiber was purchased from ZCL Composites Inc., Edmonton and had diameter varying from 10 to 20 μm. The fiber was not evenly distributed in all directions. There are more fibers oriented in quarters II and IV (referred to rolling direction) than in quarters I and III (referred to transverse direction) of Figure 2.1, at a ratio of 55% to 45%. Five layers of fiber mat were cut and prepared in order to make a FRP panel. Each layer of fiber was weighed to calculate fiber volume fraction, which will be discussed later in Section 2.4.1. All layers were stacked in the same orientation, and the applied load for the mechanical tests was always in the rolling direction. E-glass fiber has the following properties [46]: density ρ_f = 2540 kg/m^3, modulus E_f = 72.40 GPa, and UTS σ_u = 3.45 GPa.

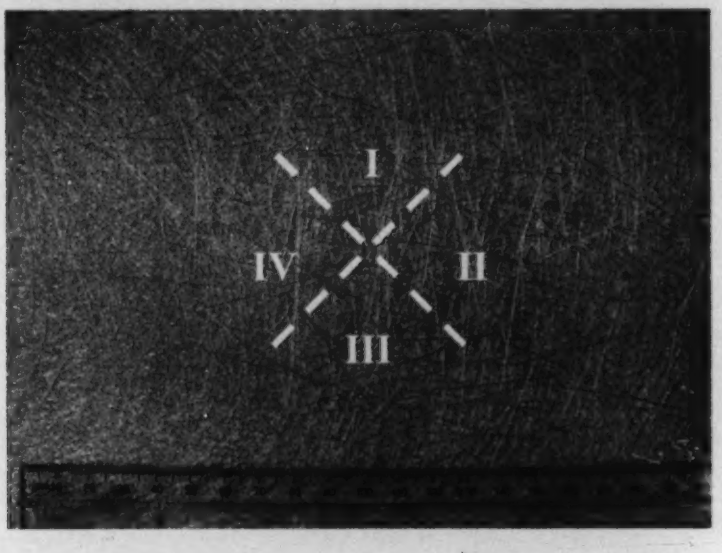

Figure 2.1. Randomly oriented fiber mat used in this study.

Glass fibers are generally made by drawing from a melt of a mixture that includes sand, limestone, and alumina. The fibers are sprayed with an organic sizing solution after they are drawn. The sizing solution contains a mixture of binders, lubricants, and coupling and antistatic agents. The binders allow the filaments to be packed in strands, lubricants prevent abrasion of filaments, and coupling agents give better adhesion between the inorganic glass fiber and the organic matrix [46]. The main function of the sizing is to lubricate the fibers to prevent them from abrading and subsequently weakening each other during the subsequent handling and weaving operations. This sizing solution evaporates when heated at high temperature. It is, therefore, necessary to determine the sizing mass in order to calculate void content in FRPs. Otherwise the void content is overestimated.

Polyester was purchased from Triple M. Fiberglass, Edmonton. Its consumption represents approximately 2.4% of the total plastic consumption and 13-21% of the total

thermoset consumption [45]. It is widely used as a matrix of FRP because it has low cost, desirable chemical and physical properties, and can be cured at room temperature [47]. Polyester-based FRP has been extensively used for study due to nature of resin transparency. However, polyester fails by brittle fracture.

Polyurethane was supplied by Resin Systems Inc. (RSI), Edmonton. Overall consumption of polyurethane represents 4% of the total for plastics or 31% of the total thermosets [45]. It is mainly used as one of powerful adhesives that enable simple joining processes. Interestingly, although polyurethane has wider application than polyester, there has not been much work done on the polyurethane-based FRP under fatigue loading. Polyurethane is believed to be a good candidate for matrix used in FRP because of its high toughness. However, its disadvantages such as higher curing temperature, higher viscosity, shorter curing time, and voids that are often created due to by-products reaction have delayed the use of polyurethane resin for fiber composites until recent years.

These polymers were used as one of the matrices with glass fiber to produce polyester- and polyurethane-based FRPs. FRPs were produced using resin transfer molding (RTM) technique. RTM is a technique to inject a low viscosity resin under low pressure into a closed mold which contains the fiber preform. The advantages of RTM are (1) less expensive than hand lay-up, (2) can be automated, and (3) does not require refrigerated storage like prepegs. The curing condition was performed at atmospheric pressure and room temperature for polyester-based FRP and elevated temperature for polyurethane-based FRPs.

2.1 Molds

There were three types of mold that were used in fabricating resin casts and FRPs. They were named mold type 1, 2 and 3. Each mold has three parts: top, middle, and bottom parts. The molds were first waxed using high-temperature mold release wax (TR Industries, California) before each use.

2.1.1 Mold Type 1

Mold type 1 was made of steel. The top and bottom parts with the same dimensions of 355 mm x 355 mm x 6.2 mm are shown in Figure 2.2. The top part had a hole with a diameter of 6.4 mm in the center from which the resin was injected. The middle part had a photo frame profile with a square plate cavity of 305 x 305 mm with different thickness of 6.4 or 3.2 mm. The outer dimensions of the middle part are the same as the top and bottom plates of 355 x 355 mm.

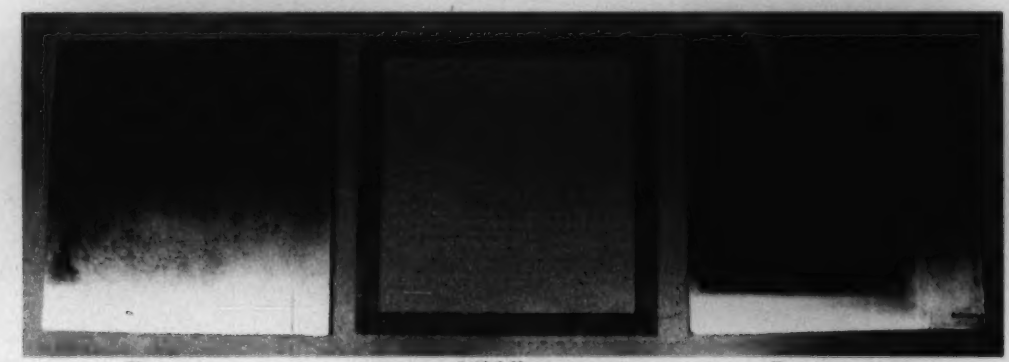

Top part Middle part Bottom part

Figure 2.2. Mold type 1.

2.1.2 Mold Type 2

Mold type 2 was also made of steel. It had the same dimensions as the top and middle parts of mold type 1. The only difference is the middle part of the mold, which was a photo frame profile with a circular plate cavity of 305 mm in diameter and a thickness of 3.2 mm. The outer dimensions are the same as the plates, as shown in Figure 2.3.

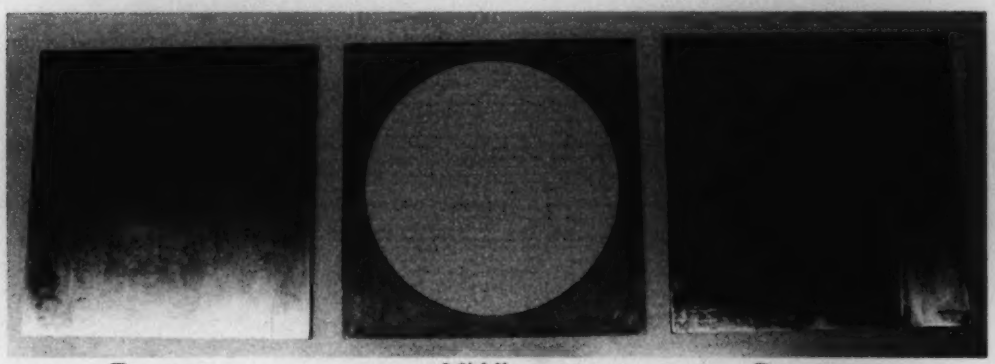

Top part Middle part Bottom part

Figure 2.3. Mold type 2.

2.1.3 Mold Type 3

Mold type 3 was made of aluminum. The top and bottom parts are plates with dimensions of 260 x 260 x 6.5 mm. The top part had a hole in the center with the same diameter as molds type 1 and 2 of 6.4 mm. Four holes, which are located 28 mm from the edges of the plate, were drilled with a 3.8 mm diameter. These holes functioned as the exit for the air when the resin was injected from the center. The middle part was a photo frame mold

with a square plate cavity of 220 x 220 mm, a thickness of 3.2 mm, and the same outer dimensions as the plates, as shown in Figure 2.4.

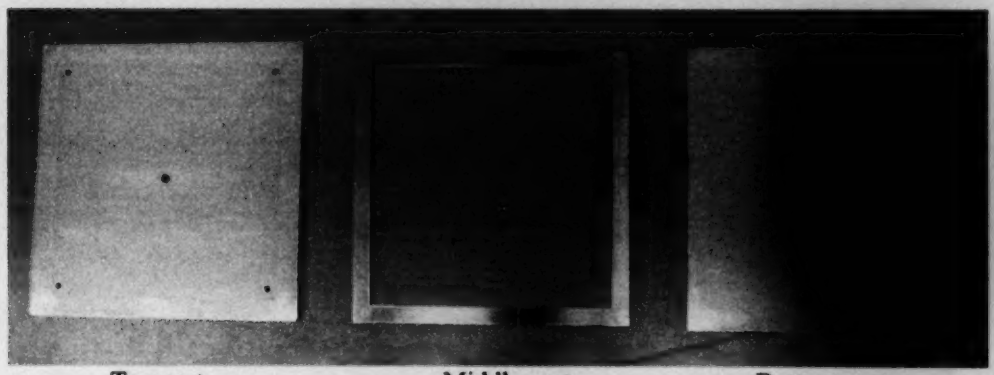

Figure 2.4. Mold type 3.

2.2 Polyester Resin Casts and Polyester-based FRP

Polyester resin casts and polyester-based FRP fabrications are divided into two categories that are resin casts for tensile and fracture toughness tests and FRP for tensile and fatigue tests.

2.2.1 Resin Casts for Tensile and Fracture Toughness Tests

For tensile test, mold type 1 with 3.2 mm-thick middle part was sealed using polyester in order to avoid leaking when the resin was poured. The position of the middle part was off by approximately 90 mm from an edge of the top and middle parts to provide a space to pour the resin vertically. The reason was to minimize resin shrinkage. The mold was then

clamped at eight different places; four at the bottom and two at the sides. The mold was then left overnight to ensure that they were bonded properly. The amount of the resin that was prepared for each cast was 400 ml. The resin was mixed and stirred with an initiator/catalyst, Methyl Ethyl Ketone Peroxide (MEKP) of 0.4% of the resin amount for 1 minute. This provided gel time of approximately 90 minutes after mixing. The resin was then poured into the mold and left overnight. The resin cast was then removed from the mold on the next day and post-cured at 70°C for 20 hours. The above procedure was also applied for resin casts used for toughness test. The only difference is the middle part of the mold used had a thickness of 6.4 mm. Hence, the resin amount had to be increased to 700 ml.

2.2.2 Polyester-based FRP for Tensile and Fatigue Tests

Mold type 2 was used in fabricating polyester-based FRP for tensile and fatigue tests. Five layers of fiber mat with a diameter of 295 mm were placed in the mold. The mold was then clamped evenly. Polyester resin was prepared with the amount of 400 ml. The catalyst with the same ratio as used in resin cast was then put into the resin and stirred for 1 minute. The polyester was poured into cartridges of injection gun and injected through a static mixer into the hole on the top part of the mold. The injection was stopped as soon as the polyester was seen dripping from the mold edges. The FRP panel inside the mold was then left overnight and post-cured on the next day at 70°C for 20 hours. The voids were found to be concentrated on the sides of the FRP panel. However, there was no

visible microscopic void in the middle of the FRP panel which can be seen later in Section 4.2.2. Only the middle section was cut to make the specimens.

2.3 Polyurethane Resin Casts and Polyurethane-based FRP

Polyurethane resin casts and polyurethane-based FRP fabrications are divided into two categories that are resin casts for tensile and fracture toughness tests and FRP for tensile and fatigue tests. Both resin casts and polyurethane-based FRP were stored for 7 days after the fabrication.

2.3.1 Resin Casts for Tensile and Fracture Toughness Tests

For tensile test, mold type 1 was used in the fabrication. The 3.2 mm-thick middle and bottom parts were glued together using polyurethane. The top part and bonded middle and bottom assembly were then clamped. The mold was then pre-heated at 50°C for 1 hour. Polyurethane resin of 200 ml was prepared and mixed with catalyst, PUL-G ISO at a ratio of 1:1 for 5 minutes. This provided gel time of approximately 15 minutes after the mixing. The mold was taken out and placed horizontally. The reason for the mold being placed horizontally was to allow air bubbles and other gasses to escape easily. The clamps and the top part were then removed. Mixed polyurethane was then poured into the mold. The mold was left overnight and cured at 120°C for 20 minutes on the next day. After approximately 5 hours, the resin cast was then removed from the mold. For toughness test, the same procedure was applied. The only difference is the mold used for

the middle part had a thickness of 6.4 mm. Hence, the amount of resin used was increased to 350 ml. This fabrication process produced polyurethane resin casts with void content of 0.55%. No shrinkage was found in the polyurethane resin casts. The specimens were taken from the central area of the panel to ensure uniform quality.

2.3.2 Polyurethane-based FRP for Tensile and Fatigue Tests

There were two types of polyurethane-based FRP, named polyurethane-based FRP type 1 (4.8% void content) and polyurethane-based FRP type 2 (2.6% void content). They were fabricated in a slightly different way.

For polyurethane-based FRP type 1, mold type 2 was used in the fabrication. Five layers of fiber mat with a diameter of 295 mm were placed in the mold. The mold was clamped and then preheated at 50°C for 1 hour. The resin and catalyst were poured separately in cartridges of injection gun at 1:1 ratio. The injection was stopped when the resin dripped from the edges of the mold. The FRP inside the mold was then left for approximately 10 minutes until it gelled at room temperature and then it was placed in an oven at 120°C for 20 minutes. The FRP panel was then taken out of the mold on the next day. Void content of 4.8% was produced using this method.

For polyurethane-based FRP type 2, mold type 3 was used in the fabrication. Five layers of fiber mat with dimensions of 215 x 215 mm were placed in the mold. The procedure and the catalyst ratio were the same as polyurethane-based FRP type 1, except the resin mixture was stirred at first for 5 minutes before placing into the cartridges. The reason for mixing was to eliminate phase separation since no heat was applied after the

injection. The amount of resin used here was larger and the mold size was smaller than those of polyurethane-based FRP type 1 in order to push the trapped air within the fibers. The FRP panel was then left overnight and cured in the oven on the next day at 120°C for 20 minutes. It was then removed from the mold after approximately 5 hours. Void content of 2.6% was produced using this method.

Eight specimens can be produced from one FRP panel, as shown in Figure 2.5. The specimens were named and arranged according to the batch number and position from A to H. A, B, C, and D are symmetric to H, G, F, and E. Figure 2.5 (a) shows the specimens arrangement for polyester-based FRP and polyurethane-based FRP type 1, and Figure 2.5 (b) shows the specimens arrangement for polyurethane-based FRP type 2.

Microvoids, which are common defects formed in the liquid molding of composite materials due to air trapped within the fiber bundles and by-product reaction, are the major contributor to property degradation. The void content in one FRP panel varied from the center to the sides due to radial resin flow. The specimens that were located close to the center had lower void content, which was also reported by other researchers [48,49]. For polyurethane-based FRP type 1, the void content ranged from the center to the sides (Figure 2.5 (a)): 4.4% (section D or E), 4.8% (section B, C, F, or G), and 5.2% (section A or H) with an average of 4.8%. For polyurethane-based FRP type 2, the void content also varied at different sections (Figure 2.5 (b)): 1.6% (section D or E), 2.4% (section B, C, F, or G), and 2.8% (section A or H) with average value of 2.3%. The difference of void content from center to the sides in polyurethane-based FRP type 2 was higher than polyurethane-based FRP type 1. Therefore, sections D and E for polyurethane-based FRP type 2 were not included in tensile specimens, but they were

used in fatigue tests. However, under fatigue loading, these specimens fractured near the neck region where the void content was about 2.6%. Therefore, for polyurethane-based FRP type 2, only specimens of around 2.6% void content were used in this study. It was reported [48] that the lower the void content is, the more significant its effect is to the mechanical properties. This is due to the exponential increase in the mechanical properties with the decrease of void content.

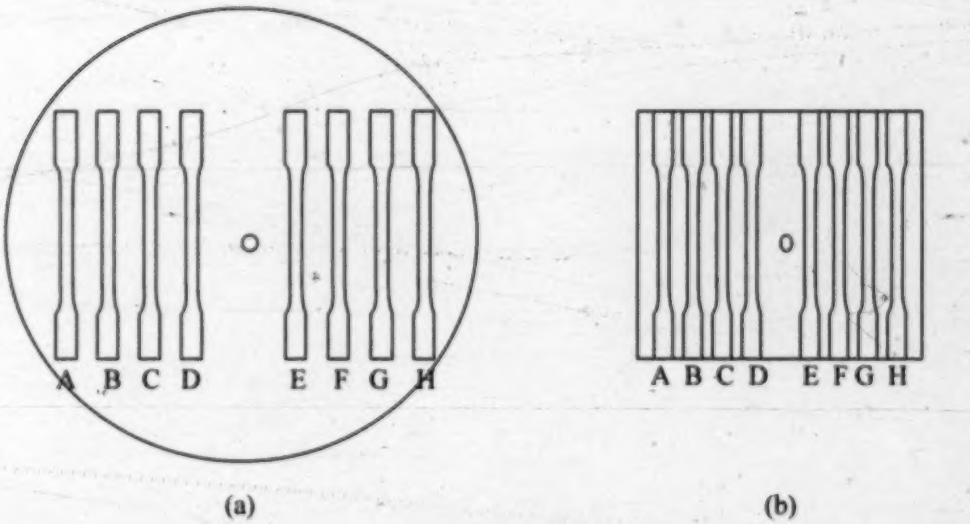

Figure 2.5. FRP panels: (a) polyester-based FRP and polyurethane-based FRP type 1 and (b) polyurethane-based FRP type 2.

2.4 Fiber Volume Fraction and Void Content Calculation

2.4.1 Fiber Volume Fraction

Fiber volume fraction, V_f of the FRPs is given by

$$V_f = \frac{v_f}{v_c} \tag{2.1}$$

where v_f and v_c are volume of fiber and composite, respectively.

Volume of the fiber, v_f is given by

$$v_f = \frac{m_f}{\rho_f} \tag{2.2}$$

where m_f is the mass of five layers of fiber mat and ρ_f is the density of the fiber (2540 kg/m^3).

Volume of the composite, v_c for polyester-based FRP and polyurethane-based FRP type 1 is given by

$$v_c = \pi r^2 t \tag{2.3}$$

where r is the radius of the cut fiber mats (147.5mm) and t is the average specimens thickness in one batch.

Volume of the composite, v_c for polyurethane-based FRP type 2 is given by

$$v_c = wlt \tag{2.4}$$

where $w = l$ which is the width or length of the cut fiber mats (215 mm) and t is the average specimens thickness in one batch. Substituting Equations (2.2) and (2.3) for polyester-based FRP and polyurethane-based FRP type 1 (or Equation (2.4) for polyurethane-based FRP type 2) to Equation (2.1), fiber volume fraction of FRPs can be determined.

It was unlikely to provide FRP with consistent quality because of the potential variation in distributions of random long-fiber mats. The fiber volume fraction was found to range from 25 to 28% for polyester-based FRP, 23 to 25% for polyurethane-based FRP

type 1, and 25 to 27% of polyurethane-based FRP type 2, as shown in Table 2.1. It was noticed that polyurethane-based FRP type 1 had lower fiber volume fraction than polyurethane-based FRP type 2 because of the thickness difference between the two FRPs. Polyurethane-based FRP type 1 and polyurethane-based FRP type 2 had average thickness of 3.43 mm and 3.12 mm, respectively. This is possibly due to higher void content that created higher internal pressure from the gasses and the larger mold area used for fabrication of polyurethane-based FRP type 1. Polyester-based FRP and polyurethane-based FRP type 2 had the same thickness, thus giving the same fiber volume fraction.

Table 2.1. Batch number, type of FRPs, type of testing, average fiber mass, and fiber volume fraction.

Batch number	Type of FRPs	Type of testing	Average fiber mass (gram)	Fiber volume fraction
Y-19	Polyester	Tensile	29.2	27%
Y-22		Tensile	28.1	26%
Y-27		Fatigue	28.1	26%
Y-29		Fatigue	27.6	25%
Y-30		Fatigue	30.1	28%
Y-18	Polyurethane type 1	Tensile	27.3	23%
Y-20		Tensile	26.9	23%
Y-21		Fatigue	29.0	25%
Y-23		Fatigue	29.1	25%
Y-26		Fatigue	27.6	23%
Y-50	Polyurethane type 2	Tensile and Fatigue	18.6	25%
Y-51		Tensile and Fatigue	18.7	26%
Y-53		Tensile and Fatigue	19.7	27%
Y-55		Fatigue	19.6	26%
Y-56		Fatigue	19.4	26%

2.4.2 Void Content of Resin Casts

Resin casts fabrication produced void-free polyester and 0.55% void content polyurethane. Small samples of polyurethane were cut from resin cast panels and their void content, V_v, was calculated as follows:

$$V_v = \frac{v_v}{v_r} \tag{2.5}$$

where v_v and v_r are volume of voids and resin cast, respectively.

Volume of the resin cast, v_r, which is the summation of volume of the matrix, v_m, and void, v_v, is given by

$$v_r = v_m + v_v$$

Dividing the above equation by v_r, it becomes

$$1 = \frac{v_m + v_v}{v_r}$$

Using Equation (2.5), we can get

$$V_v = 1 - \left(\frac{v_m}{v_r}\right)$$

Substituting volume of the matrix, $v_m = \frac{m_m}{\rho_m}$ to the above equation, it becomes

$$V_v = 1 - \left(\frac{m_m}{v_r \rho_m}\right) \tag{2.6}$$

where m_m and ρ_m are the mass of resin cast (mass of void = 0) and density of the resin which is 1250 kg/m^3. The density of the matrix was provided by RSI. Value of v_r was determined by dimension measurement.

2.4.3 Void Content of FRPs

It was mentioned earlier that polyester-based FRP is void-free microscopically, but this is not the case for polyurethane-based FRP. Void content calculation for polyurethane-based FRP is more challenging than polyurethane resin casts due to presence of the sizing. Void content calculation for the FRP conformed to ASTM standard D 3171-99 [50] using procedure G-matrix burnoff in a muffle furnace. Small sections of FRP placed in crucibles were burnt in a furnace at 500°C for 5 hours. The residuals inside the crucibles were only pure glass fibers without sizing. Hence, sizing mass was first determined by heating the fiber mats in the oven at 500°C for 5 hours to get pure fiber mass without sizing. Sizing mass and pure fiber mass are plotted and shown in Figure 2.6. The plot was best fit using a linear equation as follows:

$$m_s = 0.0459\, m_{pf} \tag{2.7}$$

This equation was later used to determine how much sizing mass at different pure fiber mass after burning the FRP samples.

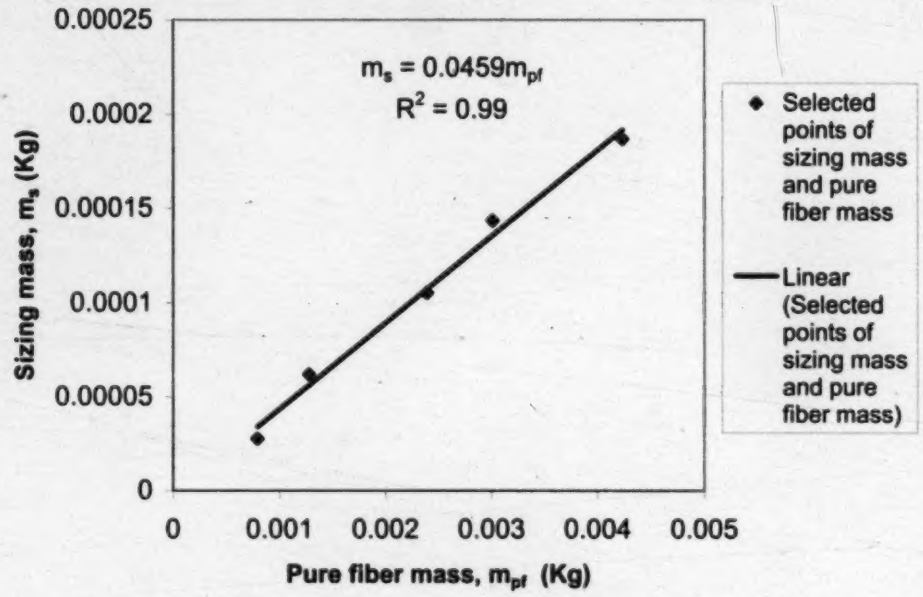

Figure 2.6. Sizing mass versus pure fiber mass.

Volume of composite, v_c, which is the summation of volume of fiber, v_f, matrix, v_m, and void, v_v, is given by

$$v_c = v_f + v_m + v_v$$

or

$$v_v = v_c - v_f - v_m \tag{2.8}$$

Dividing the above equation by v_c and substituting $\frac{v_v}{v_c}$ by V_v, it becomes

$$V_v = \frac{v_c - v_f - v_m}{v_c}$$

or

$$V_v = 1 - (\frac{v_f + v_m}{v_c}) \tag{2.9}$$

If we know v_c, v_f, and v_m, we can determine the void volume fraction of the FRP.

v_c can be calculated from $v_c = wlt$, where w = width, l = length, and t = thickness of the FRP sample.

v_f is given by

$$v_f = v_{pf} + v_s = \frac{m_{pf} + m_s}{\rho_f} \tag{2.10}$$

Pure fiber mass without sizing, m_{pf}, is the residual glass mass from burning the sample. Once this mass is known, the sizing mass, m_s, can be determined from Equation (2.7). ρ_f is the density of the fiber (2540 kg/m^3). Volume of the fiber is then determined from Equation (2.10).

Mass of the composite, m_c, is given by

$$m_c = m_{pf} + m_s + m_m$$

or

$$m_m = m_c - m_{pf} - m_s$$

Volume of the matrix is given by

$$v_m = \frac{m_m}{\rho_m} = \frac{m_c - m_{pf} - m_s}{\rho_m} \tag{2.11}$$

Since m_c, m_{pf}, m_s, and ρ_m (1250 kg/m^3) are known, m_m can be determined from Equation (2.11), so can v_m.

Substituting Equations (2.10) and (2.11) into Equation (2.9), we can get

$$V_v = 1 - \left(\frac{\frac{m_{pf} + m_s}{\rho_f} + \frac{m_c - m_{pf} - m_s}{\rho_m}}{v_c} \right)$$

Rearranging the above expression, we have

$$V_v = 1 - \left(\frac{1}{v_c} \right) \left(\left(\frac{1}{\rho_f} - \frac{1}{\rho_m} \right) (m_{pf} + m_s) + \frac{m_c}{\rho_m} \right) \tag{2.12}$$

By using Equation (2.12), it was found that the average void content of polyurethane-based FRP type 1 was 4.8% and polyurethane-based FRP type 2 was 2.6%.

3. Specimens Preparation and Test Methodology

Specimens preparation and the tests were conducted at room temperature and atmospheric pressure.

3.1 Tensile Test

Tensile tests were conducted at a close-loop servo-hydraulic 45 kN MTS model 812 material testing machine, as shown in Figure 3.1. Geometry and dimensions of the specimens conformed to the recommendation given in ASTM standard D 638-01: Type I [51], as shown in Figure 3.2 in which a set of Cartesian coordinates is given to assist in identifying the direction for microscopic observation. The applied load is in X-direction. The FRP panel was first cut to strips of 220 x 19 mm using a slow cutter. A light cutting oil was used in the process to improve the quality of the cut edges. The strips were then machined to the standard specimens using a milling machine. The edges of the specimens in the gauge section were polished using wet 600-grit sandpaper to eliminate visible defects introduced by machining.

Tensile tests were conducted at a cross-head speed of 5 mm/min. Load, strain, and displacement were recorded during the test, at a sampling rate of 25 samples/sec, for calculation of the ultimate tensile strength, strain to failure, modulus, and energy absorption. For each FRP, five specimens were randomly selected to obtain the averaged mechanical properties from minimum of 2 different batches, as shown in Table 2.1.

Figure 3.1. MTS model 812 material testing machine.

3.2 Fatigue Test

Fatigue tests were conducted using the same MTS machine as tensile test for polyester-based FRP and polyurethane-based FRP type 1. For polyurethane-based FRP type 2, fatigue tests were conducted using a 100 kN MTS model 810 material testing machine as shown in Figure 3.3. Since no standard specimen geometry and dimensions are available for fatigue test of FRP, specimens of identical dimensions as those for tensile test were used. The length for the specimens that were tested in MTS model 810 was reduced from 220 mm to 200 mm due to limited length in the grips by cutting 10 mm from each end of the specimens, but dimensions in the gauge section remained the same.

Wang and Chim [13] suggested that frequency up to 2 Hz is suitable for sheet molding compound (SMC) composite to avoid temperature rise of the specimen during

the test. An in-depth study regarding the frequency effect was conducted by Dally and Broutman [52]. They examined cross-ply and quasi-isotropic laminates and found that the temperature increase was almost unnoticeable at frequency of 1 Hz. In this study, fatigue tests were conducted at a frequency of 0.3 Hz which is far below the frequencies mentioned above, under load-controlled sinusoidal waveform, as shown in Figure 3.4.

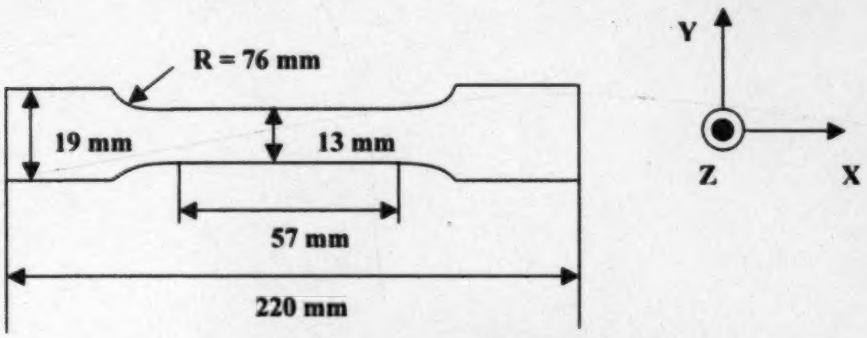

Figure 3.2. Geometry and dimensions of the specimens for tensile and fatigue tests.

Figure 3.3. MTS model 810 material testing machine.

The values of σ_{min} and σ_{max} were 0 MPa and 50% of the ultimate tensile strength of the FRPs, respectively. An additional test was conducted in polyurethane-based FRP type 2 with σ_{max} at the same absolute value of polyurethane-based FRP type 1 in order to observe the effect of void content. It should be noted that the load was firstly set to σ_{mean} before the tests started. The cycle count started after the stress reached σ_{min} in the beginning of the cycle.

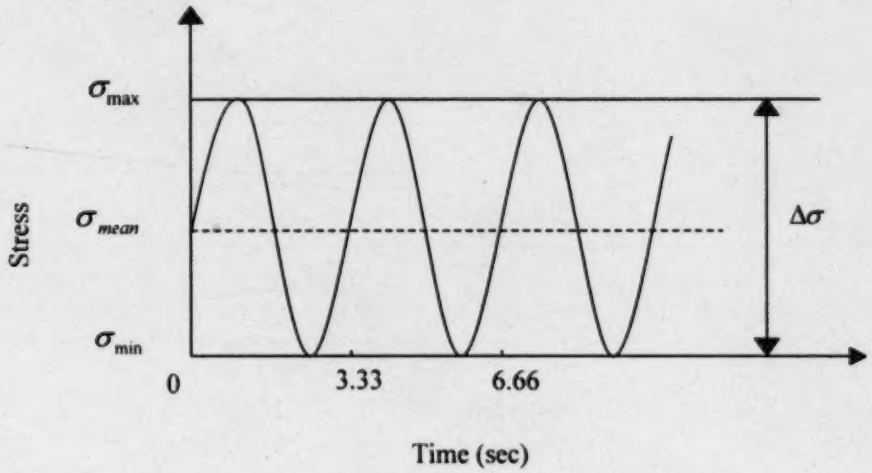

Figure 3.4. Cyclic loading function of the fatigue test.

Specimen deformation was monitored using an extensometer with initial gauge length of 25.4 mm, attached to the specimen surface in the gauge section along the width. Knife-edges of the extensometer were blunted using double-sided tape to ensure that fracture was not initiated from the contact area and no slippage took place. A computer-based data acquisition system was used to record load and displacement at a sampling rate of 240 samples/cycle during the tests for polyester-based FRP and polyurethane-based FRP type 1 and 300 samples/cycle for polyurethane-based FRP type 2 at selected

number of cycles. The data were later used to construct stress-strain curves to determine the variation in modulus and energy dissipation rate. Energy dissipation rate was defined as the energy loss in each cycle, and was determined from the area enclosed by stress-strain curve. The area was integrated using KaleidaGraph version 3.52. At least six specimens were tested for each FRP from 3 batches with slight variation in the fiber content, as shown in Table 2.1. These specimens were tested until they completely separated.

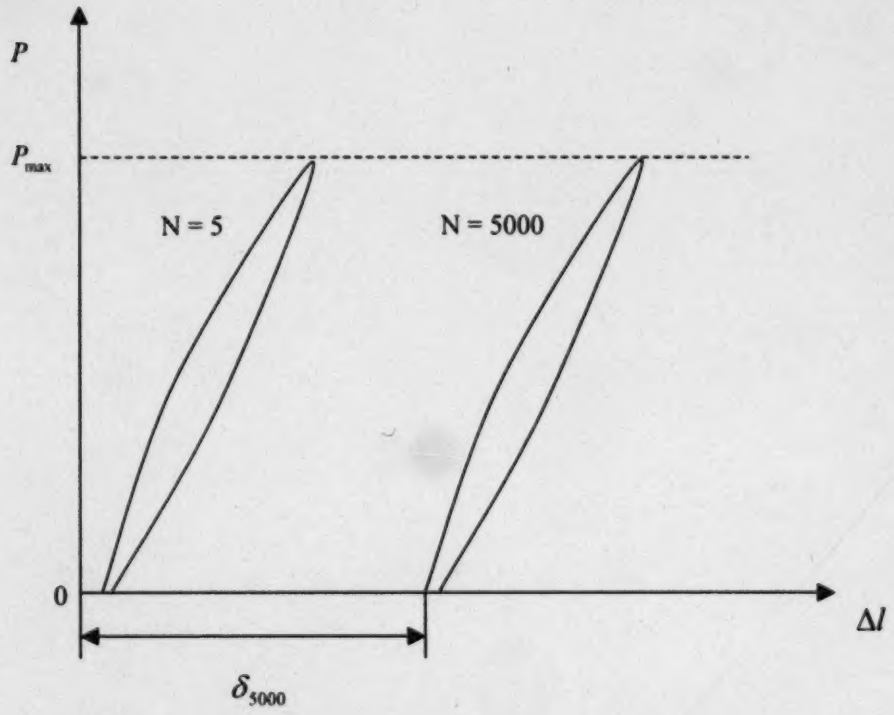

Figure 3.5. Load-displacement response under cyclic loading of the FRPs.

Preliminary tests suggested that stable cyclic response was never reached in the fatigue testing of the FRPs. The same phenomenon was also reported by several researchers [13,53]. Cumulative cyclic elongation, defined as the elongation when the

load returned to zero, was found to increase with the number of cycles due to irreversible deformation, as shown in Figure 3.5. The presence of the cumulative cyclic elongation had to be taken into account to determine the strain that responded to the loading in each cycle. This was achieved using the following equation.

$$\varepsilon_{cycles} = \frac{\Delta\delta}{l + \delta_{cycles}} \tag{3.1}$$

where ε_{cycles}, δ_{cycles}, $\Delta\delta$, and l are the true strain responding to the loading, the cumulative cyclic elongation at the measured cycles, the recorded elongation (based on the voltage output of the extensometer and the calibrated conversion factor), and the original gauge length of the extensometer (25.4 mm), respectively. It should be noted that the calculation for ε_{cycles} was only used to determine the modulus and energy dissipation rate during the cyclic loading.

3.3 Plain-strain Fracture Toughness Test

Plane-strain fracture toughness test in terms of the critical stress intensity factor, K_{IC}, was conducted on pure resins casts using a 220 kN Instron machine as shown in Figure 3.6. Geometry of the specimens conformed to the recommendation given in ASTM standard D 5045-99 [54] for single edge notch bend (SENB) test, with dimensions given in Figure 3.7. A sharp notch was machined using a milling machine up to a depth of 3 mm. A natural crack was then created by tapping with a fresh razor blade placed in the notch. The crack length, a, which was measured after the specimen fractured, satisfied the condition: $0.45 < a/W < 0.55$, or with W = 12 mm, 5.4 mm < a < 6.6 mm.

The tests were conducted at a cross-head speed of 5.08 mm/min. Load and displacement were recorded during the test, at a sampling rate of 100 samples/sec. The maximum load was later used in the calculation of K_{IC}. In order for such a result to be considered valid, according to the standard, the following criteria must be satisfied:

$$B, a, (W-a) > 2.5(K_Q/\sigma_y)^2 \tag{3.2}$$

where K_Q is the trial K_{IC} value and σ_y is the yield stress of the material for the temperature and loading rate of the test. It must be noted that σ_y is to be taken from the maximum load in a uniaxial tensile test.

Figure 3.6. 220 kN Instron machine.

K_Q can be calculated from the following equation [54]:

$$K_Q = \left(\frac{P_Q}{BW^{1/2}}\right) f(x) \tag{3.3}$$

where P_Q (N) is the maximum load at which the crack starts to propagate and factor $f(x)$ is given by

$$f(x) = 6x^{1/2} \frac{\left[1.99 - x(1-x)(2.15 - 3.93x + 2.7x^2)\right]}{(1+2x)(1-x)^{3/2}} \tag{3.4}$$

where $x = a/W$ with units in m.

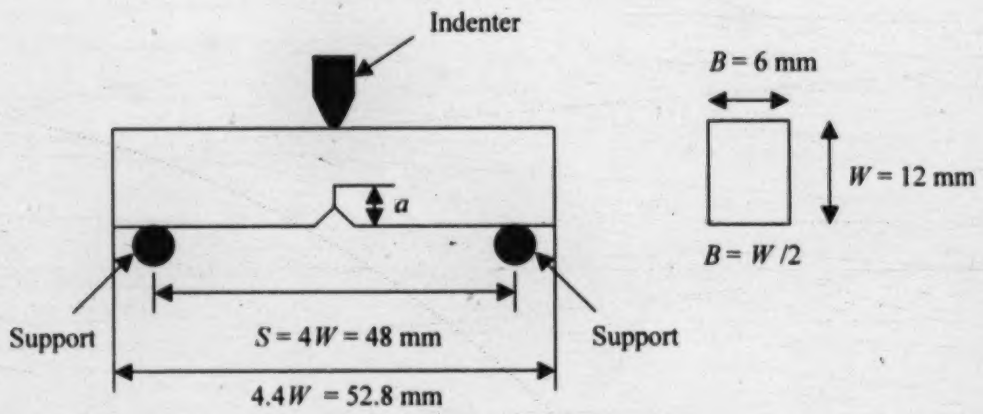

Figure 3.7. Geometry and dimensions of the specimens for fracture toughness test.

4. Results and Discussions

4.1 Tensile Test

4.1.1 Resin Casts

The tensile properties of resin casts are given in Tables 4.1 for polyester and 4.2 for polyurethane. The modulus of polyester and polyurethane was calculated from linear stress-strain curve below 10 MPa using a linear curve fit function. The modulus of polyester was found to be 3.9 GPa which was slightly higher than that of polyurethane of 3.7 GPa. However, the ultimate tensile strength, strain to failure, and energy absorbed for polyester were 47 MPa, 1.4%, and 2 J, which were lower than those of polyurethane, 80.2 MPa, 4.1%, and 10.4 J, respectively. Energy absorbed was calculated from the area under the load-displacement curve using KaleidaGraph 3.52. It should be noted that the fracture surface of polyester was near the neck of the gauge section because of the effect of stress concentration and brittleness of polyester. The stress was then calculated from the load divided by the area near the fracture surface. In polyurethane, the fracture was initiated from the void in the specimen, as shown by a white arrow in Figure 4.1.

Figure 4.1. SEM micrograph of fracture surface of pure polyurethane after tensile test.

Table 4.1. Tensile properties of polyester.*

Batch number	Energy absorbed (Joule)	Modulus (GPa)	Strain to failure (%)	Ultimate tensile strength (MPa)
E-3D	3.1	3.5	1.8	50.4
E-3G	1.5	4.0	1.3	44.5
E-3H	2.2	3.9	1.5	49.5
E-4C	1.4	4.1	1.2	42.1
E-4G	1.8	4.3	1.4	48.5
Mean	**2.0**	**3.9**	**1.4**	**47.0**
Standard deviation	**0.7**	**0.3**	**0.2**	**3.6**

* fracture near the neck for all specimens

Table 4.2. Tensile properties of polyurethane.

Batch number	Energy absorbed (Joule)	Modulus (GPa)	Strain to failure (%)	Ultimate tensile strength (MPa)
U-9E	9.4	3.7	4.2	78.9
U-9I	9.6	3.8	4.2	81.9
U-9J	9.9	3.8	4.2	81.8
U-10A	11.6	3.5	3.9	78.6
U-10B	11.6	3.6	3.9	80.1
Mean	**10.4**	**3.7**	**4.1**	**80.2**
Standard deviation	**1.1**	**0.2**	**0.2**	**1.6**

Stress-strain plot of the resin casts is shown in Figure 4.2. Solid and dashed lines represent polyester and polyurethane, respectively. Polyester was so brittle that the curve was almost linear. The polyurethane stress-strain response showed nonlinear behaviour after approximately 60 MPa and longer elongation than that of polyester.

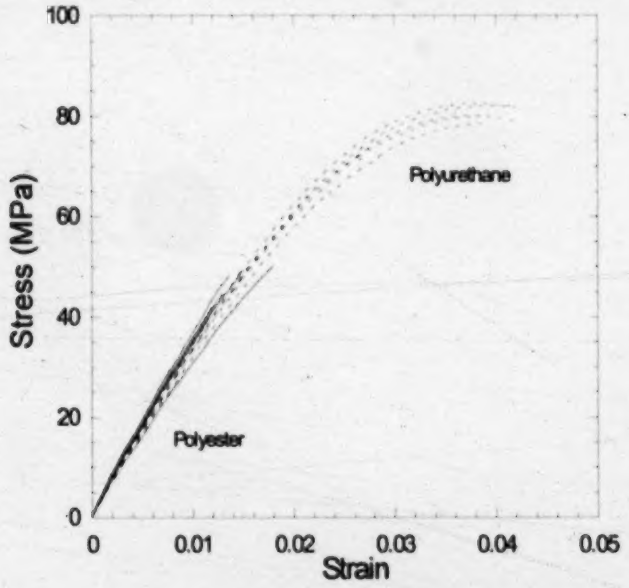

Figure 4.2. Stress-strain response of resin casts.

4.1.2 Fiber-reinforced Polymers (FRPs)

As mention earlier, tensile specimens were taken from at least two batches. Tensile tests were conducted on specimens that were randomly selected from batch Y-19 and Y-22 for polyester-based FRP, Y-18 and Y-20 for polyurethane-based type 1, and Y-50, Y-51, and Y-53 for polyurethane-based FRP type 2, as shown in Table 2.1. Tensile properties of polyester-based FRP, polyurethane-based FRP type 1, and polyurethane-based FRP type 2 are summarized in Tables 4.3, 4.4, and 4.5. It was noted that the scatter range of the mechanical properties in the FRPs was not affected by small variation in fiber volume fraction from different batches. For example, specimens Y-50 and Y-53 do not show the effect of the fiber volume fraction even if specimen Y-53 has greater fiber volume fraction. This is due to wide variation of mechanical properties in each batch because of the random fiber arrangement in the FRPs.

The average ultimate tensile strength and strain to failure for polyester-based FRP were found to be 152.4 MPa and 1.6% that were lower than those of polyurethane-based FRP of 175.1 MPa and 2.6% for type 1 and 190.4 MPa and 2.5% for type 2. The modulus was calculated for each FRP below 40 MPa using linear curve fit from stress-strain curves, which are presented in Figure 4.3. The modulus of polyester-based FRP, polyurethane-based FRP type 1, and polyurethane-based FRP 2 were found to be 12.6, 9.4, and 10.4 GPa, respectively. Lower modulus of polyurethane-based FRP was possibly due to presence of voids. Higher modulus and ultimate tensile strength for the polyurethane type 2 were expected due to lower void content, as compared to polyurethane-based FRP type 1. It was believed that with no void presence, the modulus

of polyurethane-based FRP would come close to that of polyester-based FRP, similar to that in resin cast. Energy absorbed during the tensile test was found to be 8.8, 15, and 15.3 J for polyester-based FRP, polyurethane-based FRP type 1, and polyurethane-based FRP type 2, respectively. Overall, the tensile test results suggest that the polyurethane-based FRP were tougher than polyester-counter part, with higher ultimate tensile strength and ductility.

The effect of voids on the ultimate tensile strength and modulus was reported by Olivero et al. [48]. They examined chopped strand glass mats reinforced epoxy using packing pressure and RTM technique that created void content ranging from 0.32 to 0.72%. They observed an exponential decrease in both tensile strength and modulus with increase of void content. Both stiffness and tensile strength were measured to decrease by 14 and 13%, respectively. However, they did not report the effect of voids on the strain to failure. The strain to failure was not affected by 2.2% difference in the void content in this study.

Table 4.3. Tensile properties of polyester-based FRP.

Batch number	Energy absorbed (Joule)	Modulus (GPa)	Strain to failure (%)	Ultimate tensile strength (MPa)
Y-19G	9.5	13.7	1.7	159.4
Y-22C	7.4	12.0	1.5	144.6
Y-22E	8.9	12.8	1.5	152.7
Y-22G	8.3	12.2	1.5	146.2
Y-22H	10.1	12.1	1.7	159.2
Mean	**8.8**	**12.6**	**1.6**	**152.4**
Standard deviation	**1.1**	**0.7**	**0.1**	**7.0**

Table 4.4. Tensile properties of polyurethane-based FRP type 1.

Batch number	Energy absorbed (Joule)	Modulus (GPa)	Strain to failure (%)	Ultimate tensile strength (MPa)
Y-18A	15.8	9.5	2.8	180.3
Y-18H	16.5	9.5	2.6	182.7
Y-20C	14.6	9.8	2.4	173.4
Y-20D	15.1	9.3	2.6	176.7
Y-20F	13.3	9.0	2.5	162.3
Mean	**15.0**	**9.4**	**2.6**	**175.1**
Standard deviation	**1.2**	**0.3**	**0.2**	**7.9**

Table 4.5. Tensile properties of polyurethane-based FRP type 2.

Batch number	Energy absorbed (Joule)	Modulus (GPa)	Strain to failure (%)	Ultimate tensile strength (MPa)
Y-50C	16.8	10.4	2.7	196.7
Y-50G	13.4	10.1	2.2	179.3
Y-51A	16.4	10.4	2.6	197.3
Y-53B	15.4	10.3	2.5	186.7
Y-53G	14.4	10.6	2.6	192.2
Mean	**15.3**	**10.4**	**2.5**	**190.4**
Standard deviation	**1.4**	**0.2**	**0.2**	**7.6**

Figure 4.3 shows the stress-strain plot of the FRPs. Solid, dashed lines, and dotted lines represent polyester-based FRP, polyurethane-based FRP type 1 and polyurethane-based FRP type 2, respectively. The tensile-fractured surface in the FRPs was ensured to be within the extensometer knife-edges. The nonlinearity of polyester- and polyurethane-based FRPs was noticed.

The data shown above for tensile properties of resin casts and FRPs indicate that there is a definite correlation between certain cast resin properties and the strength of the

corresponding composites tested under static loading. It was clearly demonstrated that the performance of FRPs is improved with the improvement of resin cast properties.

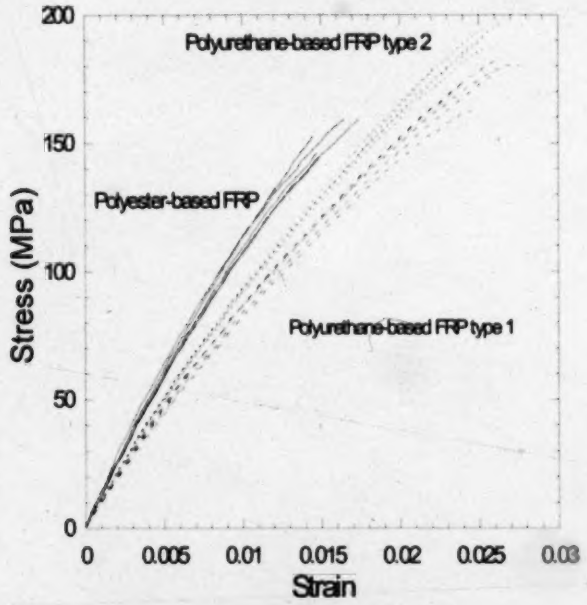

Figure 4.3. Stress-strain response of FRPs.

4.1.3 Macroscopic and Microscopic Observations

Representative photographs viewed in Z-direction (referred to Figure 3.2) of tensile-fractured specimens are presented in Figures 4.4 (a) for polyester-based FRP, (b) for polyurethane-based FRP type 1, and (c) for polyurethane-based FRP type 2. The load was applied in the horizontal direction for all images presented in this thesis. It is apparent that different fracture behaviour exists between the two FRPs. For the polyester-based FRP, some fibers still connected the two halves of the fractured specimens; while

for the polyurethane-based FRP, the specimens were completely separated into two halves. The two types of polyurethane-based FRP showed the same fracture behaviour.

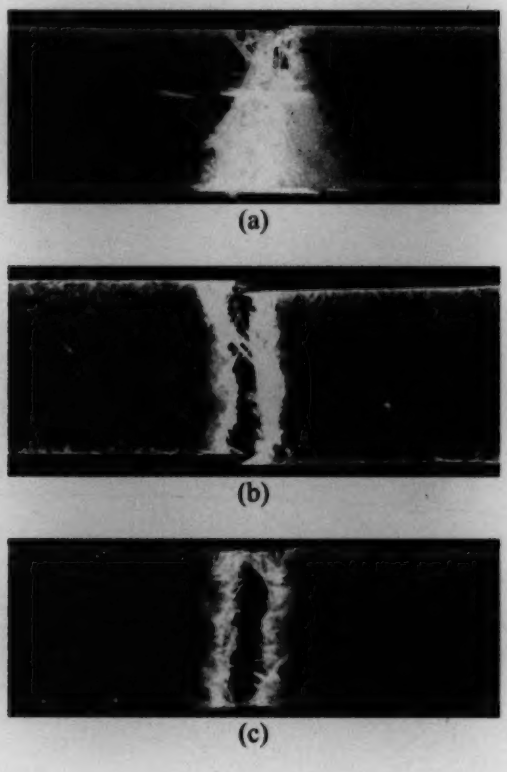

Figure 4.4. Images of tensile-fractured specimens: (a) polyester-based FRP, (b) polyurethane-based FRP type 1, and (c) polyurethane-based FRP type 2.

Micrographs near the fracture surface at high magnification that were viewed in Y-direction are shown in Figures 4.5 (a) for polyester-based FRP, (b) for polyurethane-based FRP type 1, and (c) for polyurethane-based FRP type 2. Many vertical cracks, ending at the fiber bundles, are clearly visible in the resin-rich region in Figure 4.5 (a), but very few such cracks exist in the polyurethane-based FRP and are hardly visible in Figures 4.5 (b) and (c) except in regions very close to the fracture surface. The significant

number of such cracks in the polyester-based FRP may have caused early fracture of the specimen, thus contributing to its low ultimate tensile strength and ductility.

(a)

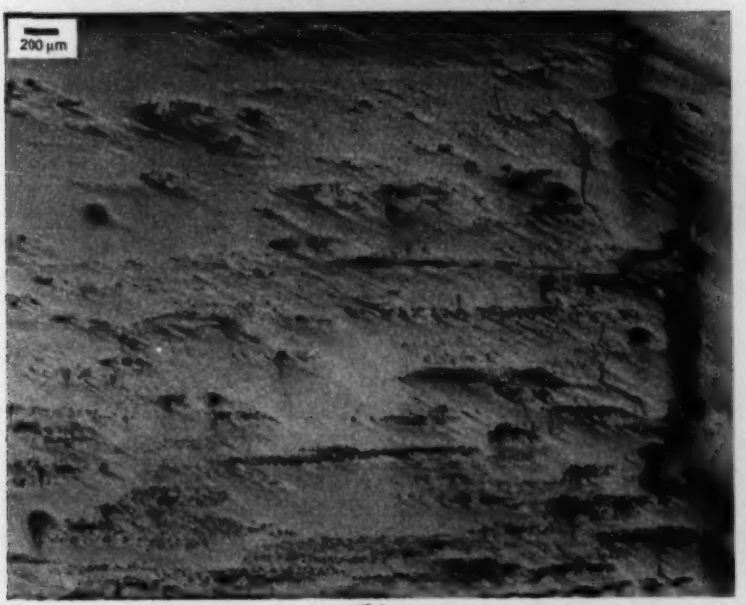

(b)

(continued...)

(c)

Figure 4.5. Micrographs viewed in Y-direction (referred to Figure 3.2) for tensile-fractured specimens near the fracture surface: (a) polyester-based FRP, (b) polyurethane-based FRP type 1, and (c) polyurethane-based FRP type 2.

Macroscopic and microscopic observations suggest that the fracture in polyester-based FRP is mostly dominated by interfacial and matrix cracks. On the other hand, the fracture in polyurethane-based FRP showed only small cracks near the fracture surface. This suggests that the bonding between fiber and matrix for polyurethane-based FRP was much better than that of polyester-based FRP.

4.2 Fatigue Test

4.2.1 Mechanical Properties under Fatigue Loading

From tensile test results, polyester-based FRP, polyurethane-based FRP type 1, and polyurethane-based FRP type 2 were cyclically tested in the range of 0-76.2 MPa, 0-87.6 MPa, and 0-95.2 MPa and 0-87.6 MPa. Three parameters were monitored during the fatigue testing i.e. cumulative strain ($\frac{\delta}{l}$, where δ and l are the cumulative cyclic elongation at the measured cycles and original length of strain gauge, 25.4 mm), modulus, and energy dissipation rate. The fatigue lifetime and the last recorded cycles by the pre-programmed data acquisition were shown in second column of Tables 4.6, 4.7, 4.8, and 4.9 for polyester-based FRP, polyurethane-based FRP type 1, polyurethane-based FRP type 2 at 0-95.2 MPa, and polyurethane-based FRP type 2 at 0-87.6 MPa, respectively. The third column shows the minimum and maximum strains at the last recorded cycles. In general the cumulative strains of polyurethane-based FRP was higher than that of polyester-based FRP. As mentioned earlier in Section 2.3.2, specimens in positions D and E for polyurethane-based FRP type 2 fractured near the neck due to higher void content in this area.

The fatigue lifetime at 50% UTS of polyester-based FRP ranged from 15,000 to 55,000 cycles, polyurethane-based FRP type 1 ranged from 30,000 to 85,000 cycles, and polyurethane-based FRP type 2 ranged from 25,000 to 61,000 cycles. Polyurethane-based FRP showed longer fatigue lifetime than polyester-based FRP even when cycled at higher absolute stress levels. The additional tests for polyurethane-based FRP type 2 cycled at the same absolute stress level of 0-87.6 MPa showed longer fatigue lifetime than polyurethane-based FRP type 1, ranging from 46,000 to more than 300,000 cycles. It was obvious that lower void content lengthened the fatigue lifetime.

Table 4.6. Fatigue lifetime, last recorded cycles, and cumulative strains of polyester-based FRP cycled at 0-76.2 MPa.

Batch number	Fatigue lifetime and last recorded cycles	Minimum and maximum cumulative strains (%)
Y-27E	21,745 and 21,000	0.16 and 0.94
Y-27F	15,166 and 15,000	0.14 and 1.05
Y-29B	20,130 and 20,000	0.16 and 1.07
Y-29C	47,248 and 45,000	0.24 and 1.25
Y-30B	52,897 and 50,000	0.11 and 0.85
Y-30D	55,715 and 55,000	0.11 and 0.80

Table 4.7. Fatigue lifetime, last recorded cycles, and cumulative strains of polyurethane-based FRP type 1 at 0-87.6 MPa.

Batch number	Fatigue lifetime and last recorded cycles	Minimum and maximum cumulative strains (%)
Y-21F	39,195 and 35,000	0.23 and 1.24
Y-21G	30,095 and 30,000	0.23 and 1.14
Y-23D	40,555 and 40,000	0.26 and 1.34
Y-23E	53,576 and 50,000	0.29 and 1.35
Y-26E	85,300 and 85,000	0.29 and 1.32
Y-26G	30,769 and 30,000	0.24 and 1.34

Table 4.8. Fatigue lifetime, last recorded cycles, and cumulative strains of polyurethane-based FRP type 2 at 0-95.2 MPa.

Batch number	Fatigue lifetime and last recorded cycles	Minimum and maximum cumulative strains (%)
Y-50A	39,001 and 39,000	0.23 and 1.41
Y-50D	30,287 and 30,000	0.29 and 1.38
Y-51C	61,311 and 61,000	0.26 and 1.34
Y-51E	50,793 and 50,000	0.27 and 1.39
Y-55A	25,876 and 25,000	0.23 and 1.37
Y-55E	25,510 and 25,000	0.26 and 1.37

Table 4.9. Fatigue lifetime, last recorded cycles, and cumulative strains of polyurethane-based FRP type 2 at 0-87.6 MPa.

Batch number	Fatigue lifetime and last recorded cycles	Minimum and maximum cumulative strains (%)
Y-53D	135,553 and 135,000	0.28 and 1.31
Y-53E	69,882 and 69,000	0.22 and 1.18
Y-55B	300,000 and 300,000*	0.19 and 1.08
Y-55C	46,058 and 46,000	0.19 and 1.22
Y-56A	100,825 and 100,000	0.30 and 1.36
Y-56G	50,833 and 50,000	0.23 and 1.25

Minimum and maximum cumulative strains versus number of cycles starting from 50 cycles of FRPs are shown in Figures 4.6 (a) for polyester-based FRP, (b) for polyurethane-based FRP type 1, (c) for polyurethane-based FRP type 2 at 0-95.2 MPa, and (d) for polyurethane-based FRP type 2 at 0-87.6 MPa. These figures show increasing minimum and maximum cumulative strains with increase of the number of cycles. The cumulative strains of FRPs showed significant increase in the early cycles. After those cycles, the rate of increase was reduced with polyester-based FRP at a higher rate than that of polyurethane-based FRP. A wide scatter range of maximum strain in polyester-based FRP was observed, possibly due to damage in matrix which occurred after 1,000 cycles (Section 4.2.2).

* not fracture

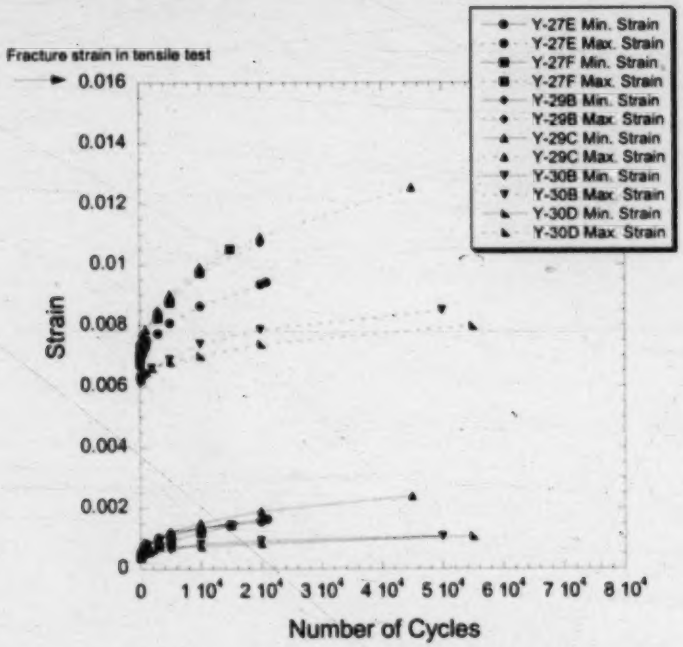

(a)

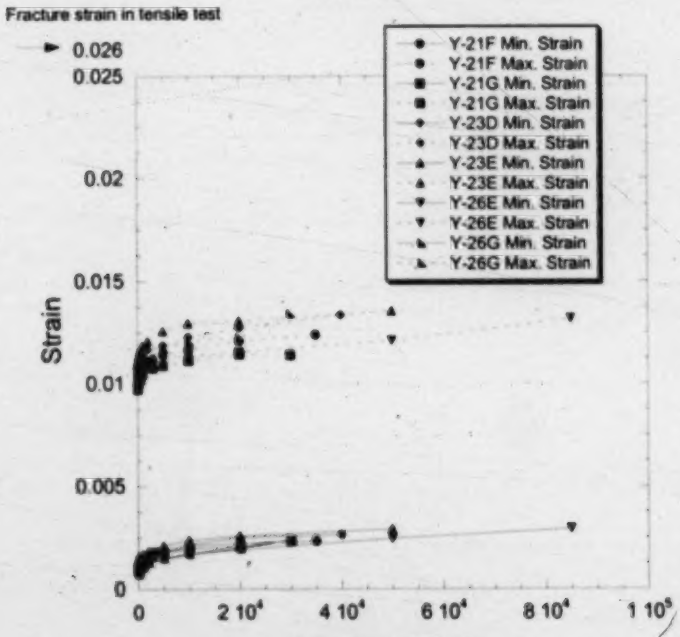

(b)

(continued...)

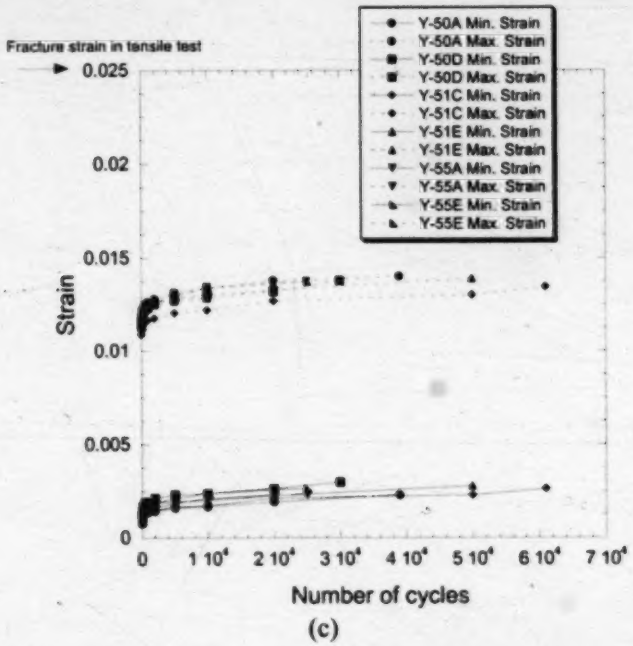

(c)

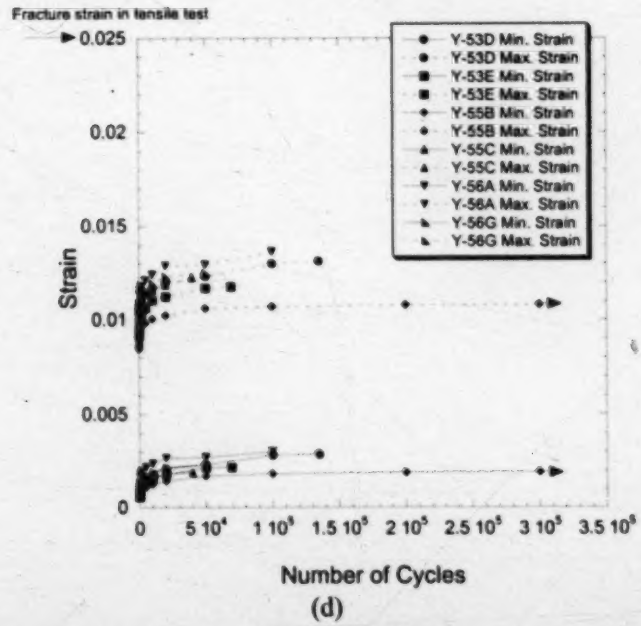

(d)

Figure 4.6. Linear plots of cumulative strains versus number of cycles: (a) polyester-based FRP, (b) polyurethane-based FRP type 1, (c) polyurethane-based FRP type 2 at 0-95.2 MPa, and (d) polyurethane-based FRP type 2 at 0-87.6 MPa.

By extending the curves up to the cycles for fatigue fracture, it was observed that the maximum cumulative strain at the end of fatigue lifetime did not occur at the same strain to failure of the tensile tests of the FRPs. Maximum cumulative strain in these FRPs under fatigue loading was lower than strain to failure of the FRPs in tensile tests. It was suggested [39] that unnotched fatigue failures are separated into two fatigue failure conditions: (1) cumulative damage failures, which accumulate creep strain until the specimen breaks into two halves, much like chopped strand materials, and (2) crack initiation and propagation dominate the lifetime. In case (1), failure occurs when the maximum cumulative strain reaches a critical value that is similar to static ultimate strain. In case (2), failure occurs at maximum cumulative strain which decreases as the cyclic stress level decreases. The latter is consistent with a crack propagation model in which the rate of crack extension is a function of the stress intensity factor, K_I, and final fracture occurs when the most severe crack reaches a certain critical length sufficient to cause catastrophic failure [55]. This should be in stress-controlled phenomenon since K_I is a function of stress and crack length only which is given by

$$K_I = Y(a/w)\sigma\sqrt{\pi a} \qquad (4.1)$$

However, Equation (4.1) cannot be applied directly to the composite due to limitation of the theory, which can only be applied to isotropic and homogeneous materials. From the above explanation, it can be concluded that polyester- and polyurethane-based FRPs are of the second case, that is, failure was due to crack initiation and propagation.

Semi-logarithmic plots of absolute modulus versus number of cycles for these FRPs were plotted and are shown in Figure 4.7. Figures 4.7 (a), (b), (c), and (d) show the modulus degradation of polyester-based FRP, polyurethane-based FRP type 1,

polyurethane-based FRP type 2 at 0-95.2 MPa, and polyurethane-based FRP type 2 at 0-87.6 MPa. The plots suggest that the modulus decreased with the increase of the number of cycles. This is an indication of fatigue damage in the FRPs, as reported in the past [8,12-14,17,18]. Variation of the absolute modulus for each FRP is possibly because the variation of fiber distributions and content among the batches. In Figure 4.7 (d), the specimen Y-55B did not fracture even after 300,000 cycles, and showed the highest absolute modulus. Its modulus was exceptionally higher than the others possibly because of more fiber aligned along the loading direction.

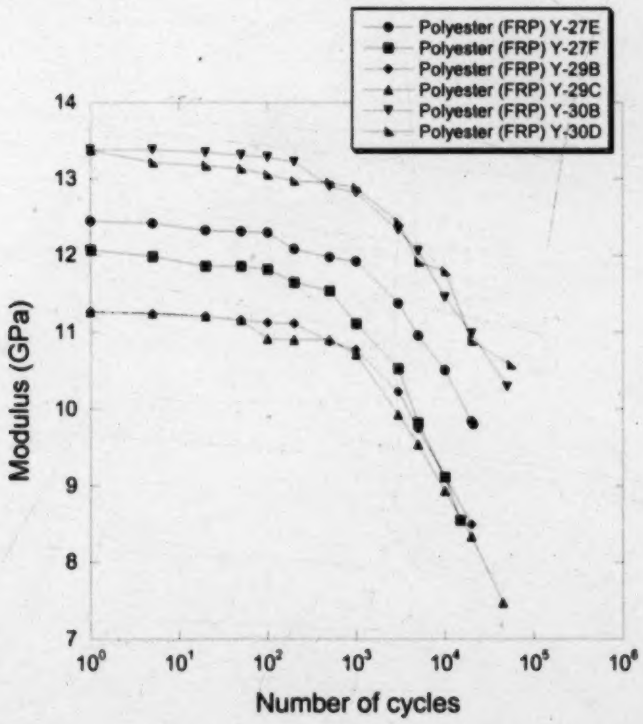

(a)

(continued...)

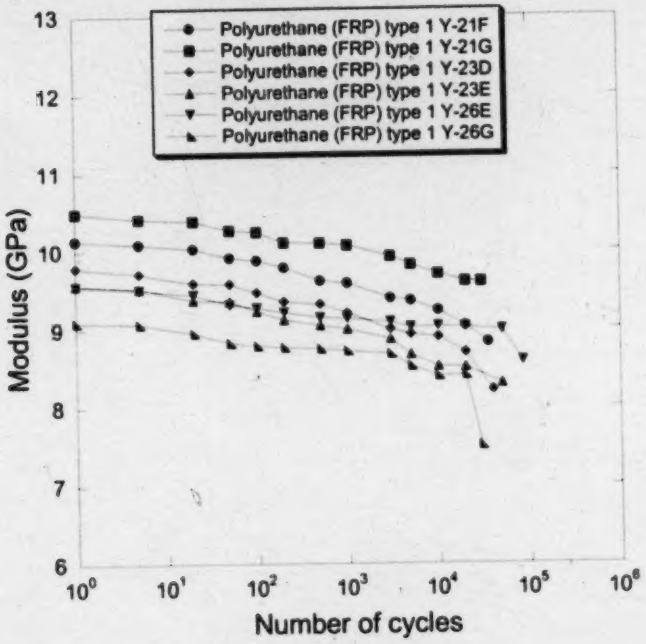
Polyurethane (FRP) type 1 Y-21F
Polyurethane (FRP) type 1 Y-21G
Polyurethane (FRP) type 1 Y-23D
Polyurethane (FRP) type 1 Y-23E
Polyurethane (FRP) type 1 Y-26E
Polyurethane (FRP) type 1 Y-26G
Modulus (GPa)
Number of cycles

(b)

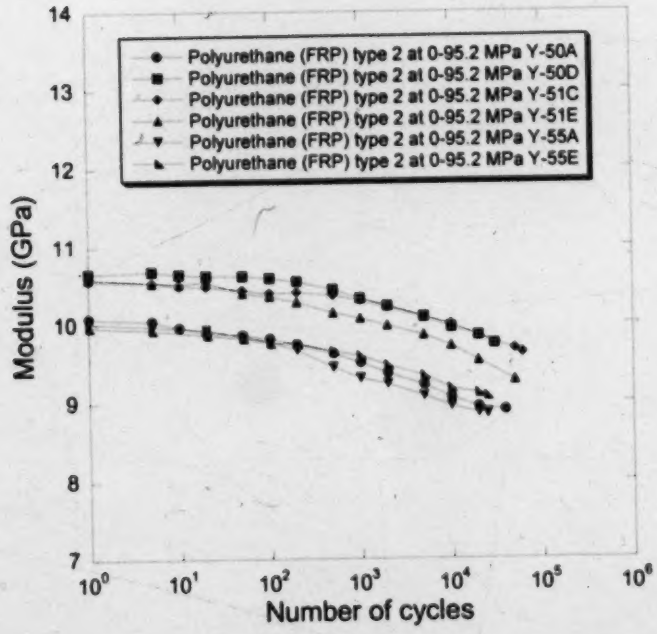
Polyurethane (FRP) type 2 at 0-95.2 MPa Y-50A
Polyurethane (FRP) type 2 at 0-95.2 MPa Y-50D
Polyurethane (FRP) type 2 at 0-95.2 MPa Y-51C
Polyurethane (FRP) type 2 at 0-95.2 MPa Y-51E
Polyurethane (FRP) type 2 at 0-95.2 MPa Y-55A
Polyurethane (FRP) type 2 at 0-95.2 MPa Y-55E
Modulus (GPa)
Number of cycles

(c)

(continued...)

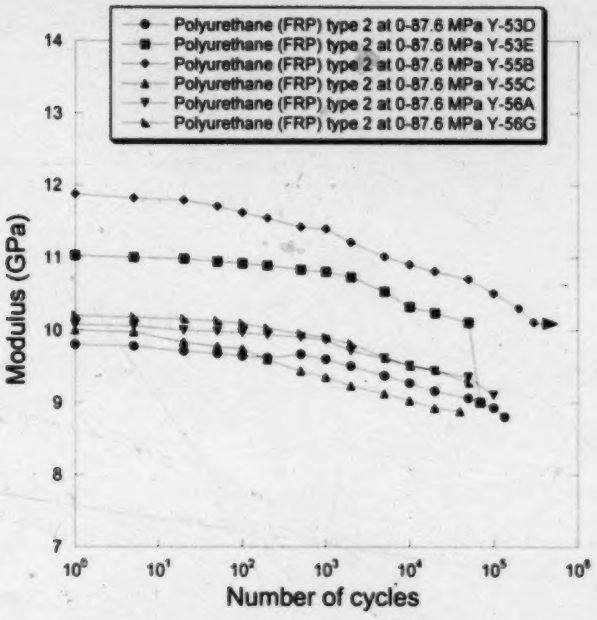

(d)

Figure 4.7. Semi-logarithmic plots of absolute modulus versus number of cycles: (a) polyester-based FRP, (b) polyurethane-based FRP type 1, (c) polyurethane-based FRP type 2 at 0-95.2 MPa, and (d) polyurethane-based FRP type 2 at 0-87.6 MPa.

Scattering of the modulus can be reduced by plotting normalized modulus (defined as the ratio of the modulus to that measured in the 1st loading cycle) versus number of cycles. Semi-logarithmic plots of normalized modulus versus the number of cycles are shown in Figures 4.8 (a), (b), (c), and (d) for polyester-based FRP, polyurethane-based FRP type 1, polyurethane-based FRP type 2 at 0-95.2 MPa, and polyurethane-based FRP type 2 at 0-87.6 MPa. These plots clearly show that for polyester-based FRP, the normalized modulus dropped significantly after about 1000 cycles of fatigue loading; while the drop for the polyurethane-based FRP type 1 and polyurethane-based FRP type 2 remained minor until near the end of the fatigue lifetime

when it also dropped significantly for polyurethane-based FRP type 1 and dropped slightly for polyurethane-based FRP type 2. It was also noticed that modulus values tended to disperse widely after 1,000 cycles, possibly because the commencement of certain damage development varied among the specimens. Nevertheless, the trend of modulus change remains the same among specimens of the same FRP.

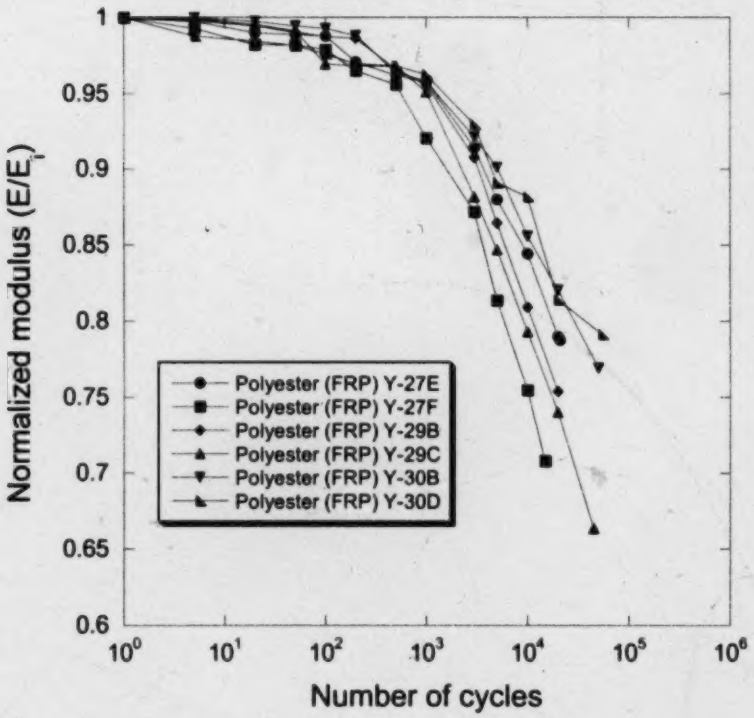

(a)

(continued...)

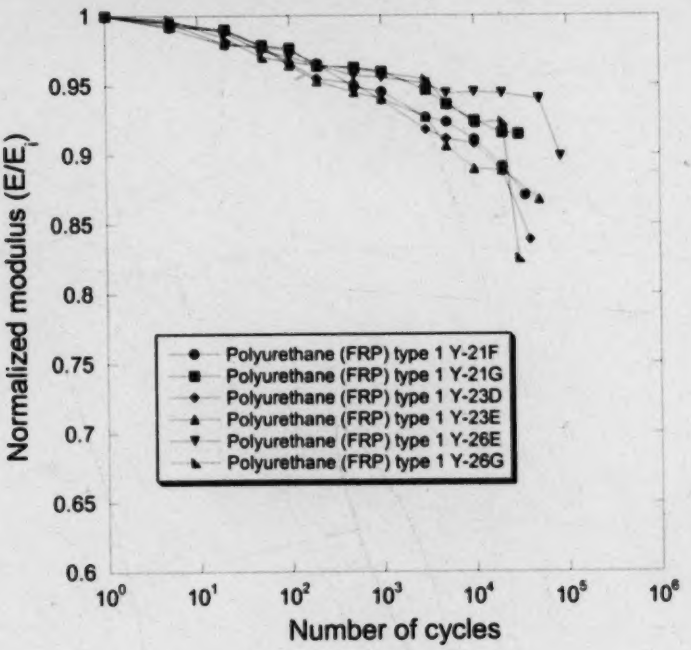
Normalized modulus (E/E$_i$)
Number of cycles
Polyurethane (FRP) type 1 Y-21F
Polyurethane (FRP) type 1 Y-21G
Polyurethane (FRP) type 1 Y-23D
Polyurethane (FRP) type 1 Y-23E
Polyurethane (FRP) type 1 Y-26E
Polyurethane (FRP) type 1 Y-26G

(b)

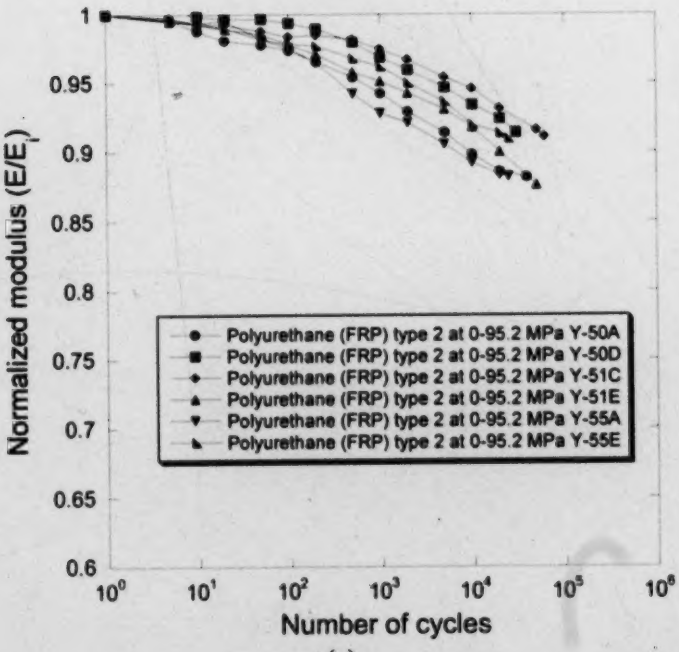
Normalized modulus (E/E$_i$)
Number of cycles
Polyurethane (FRP) type 2 at 0-95.2 MPa Y-50A
Polyurethane (FRP) type 2 at 0-95.2 MPa Y-50D
Polyurethane (FRP) type 2 at 0-95.2 MPa Y-51C
Polyurethane (FRP) type 2 at 0-95.2 MPa Y-51E
Polyurethane (FRP) type 2 at 0-95.2 MPa Y-55A
Polyurethane (FRP) type 2 at 0-95.2 MPa Y-55E

(c)

(continued...)

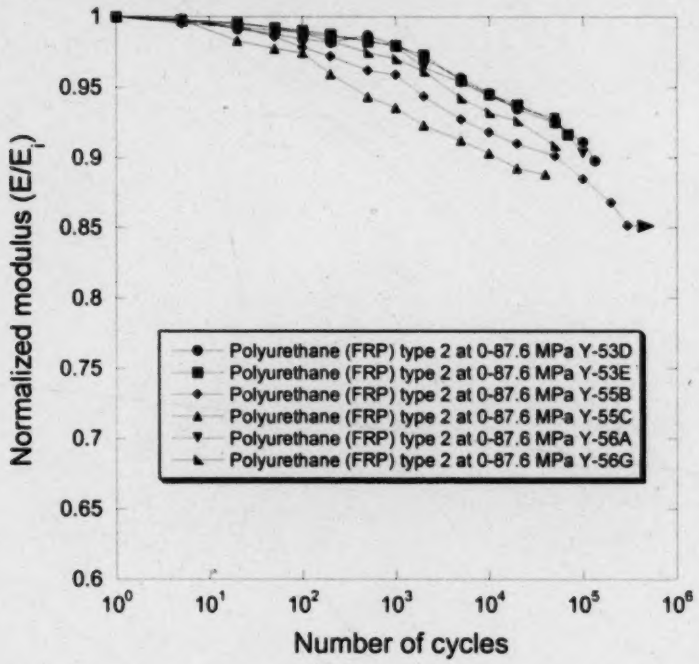

(d)

Figure 4.8. Semi-logarithmic plots of normalized modulus versus number of cycles: (a) polyester-based FRP, (b) polyurethane-based FRP type 1, (c) polyurethane-based FRP type 2 at 0-95.2 MPa, and (d) polyurethane-based FRP type 2 at 0-87.6 MPa.

Two specimens of each FRP that represent its typical normalized modulus degradation curves in Figure 4.8 are plotted in Figures 4.9 (a) and (b) for semi-logarithmic and linear plots for easy comparison. Figure 4.9 (a) shows that in the early cycles up to about 1000 cycles, polyurethane-based FRP type 1 had slightly lower normalized value than that of polyester-based FRP. By reducing the void content to 2.6%, the normalized modulus drop of polyurethane-based FRP type 2 was almost the same as polyester-based FRP in the early cycles. Afterwards, the normalized modulus for polyurethane-based FRP showed less significant drop than that of the polyester-based

FRP. Comparing polyurethane-based FRP type 1 and type 2 at the same stress level, type 1 had significant modulus drop probably due to its higher void content. The figure also shows that the trend of modulus degradation for polyurethane-based FRP type 2 at 0-95.2 MPa is slightly more significant than that at 0-87.6 MPa. This finding is consistent with Wang's results [13].

Figure 4.9 (b) is a linear plot of modulus degradation versus number of cycles, which shows a different perspective from that given in Figure 4.9 (a). It shows that within the first 1,000 cycles, FRPs had a significant modulus drop. Soon afterwards, polyester-based FRP showed a further significant drop, but at a slower rate, while the polyurethane-based FRP tended to have the modulus remain at a constant level. Only at the end of the fatigue lifetime did the polyurethane-based FRP show a significant decrease in the modulus.

Energy dissipation rate is presented in Figure 4.10 as a function of the logarithmic number of cycles. The energy dissipation rate was used to detect damage during the early stage of fatigue test [18]. Without any heat loss, as expected for low-frequency fatigue test at 0.3 Hz, the energy dissipation rate represents the irrecoverable energy that is used for generating permanent deformation and damage in the FRPs, such as local delamination, plastic flow of the matrix, friction energy loss, fiber pull out, etc. Damage mechanisms contribute to crack development and degradation of mechanical properties during fatigue loading.

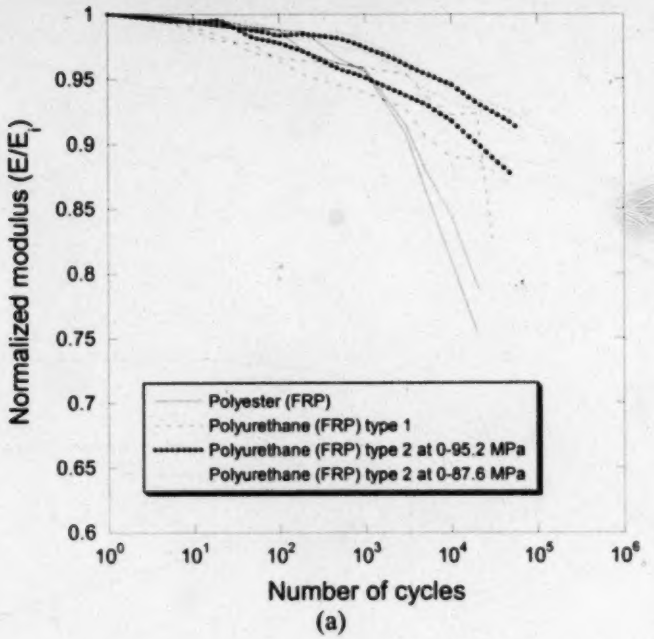

(a)

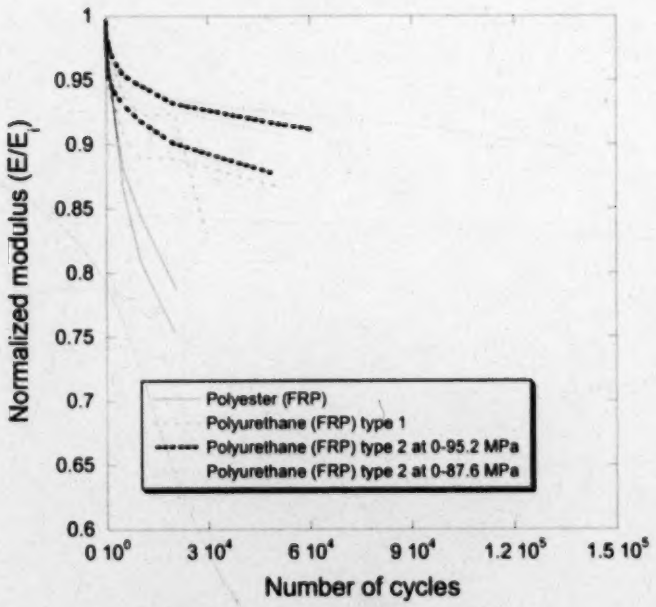

(b)

Figure 4.9. Typical plots of normalized modulus versus number of cycles of FRPs: (a) semi-logarithmic plot and (b) linear plot.

Figure 4.10 (a) suggests that for polyester-based FRP, the energy dissipation rate increased significantly after about 1,000 cycles. It has been suggested [3,55] that increase in energy dissipation rate could be caused by friction between fiber and matrix and/or fiber reorientation behind the crack tips because the fibers are not in parallel with the loading direction. This provides a mechanical interlocking across the matrix crack as well as a resistance to fiber pull-out along their length by frictional forces. Thus, although the fibers might have debonded and matrix cracked, there could still be a substantial work required for the crack opening. This could provide an explanation for the phenomenon in Figure 4.10 (a).

On the other hand, in the case of polyurethane-based FRP, a slight increase of energy dissipation rate occurred in the early stage of the fatigue loading, up to approximately 1,000 cycles, after which the trend was reversed, as shown in Figures 4.10 (b), (c), and (d) for polyurethane-based FRP type 1, polyurethane-based FRP type 2 at 0-95.2 MPa, and polyurethane-based FRP type 2 at 0-87.6 MPa. A small increase of the energy dissipation rate could be observed at the end of fatigue life for polyurethane-based FRP in some specimens.

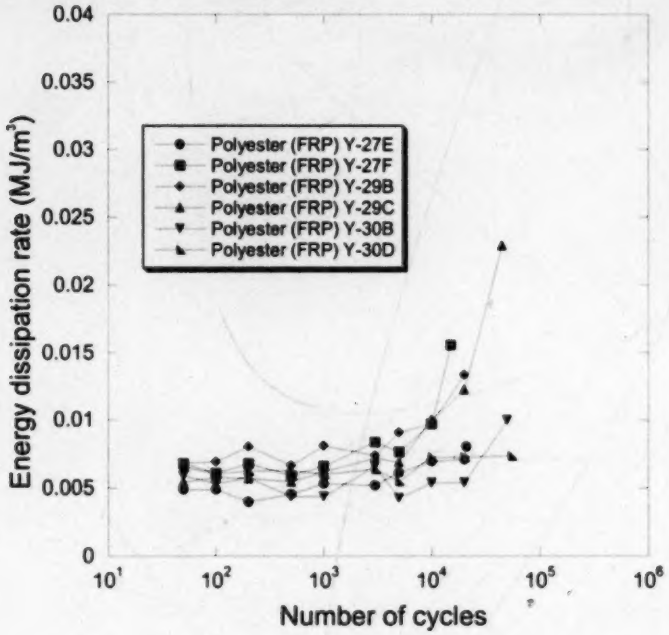

(a)

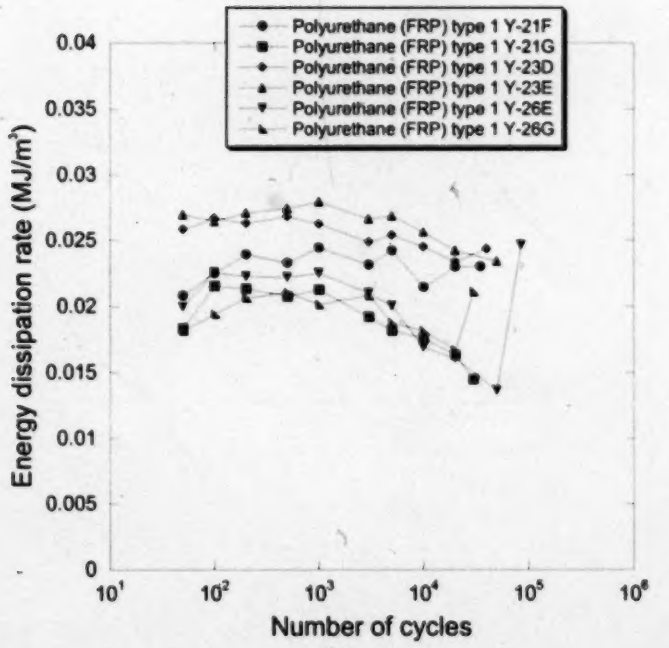

(b)

(continued...)

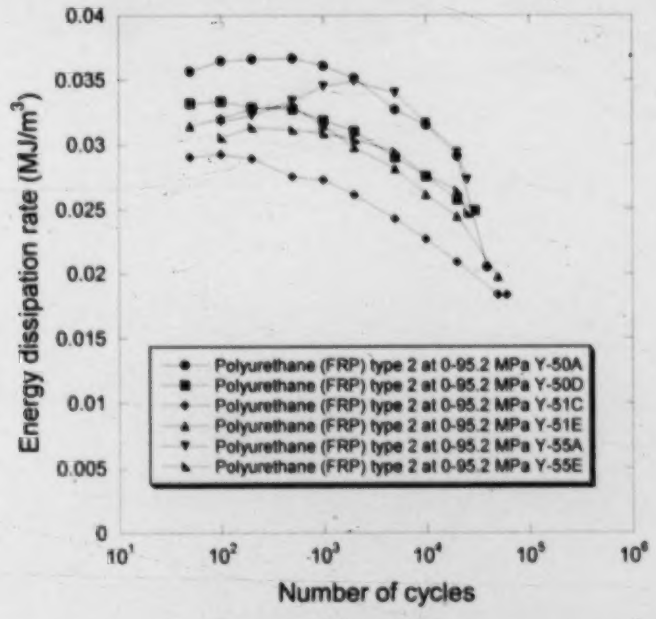

(c)

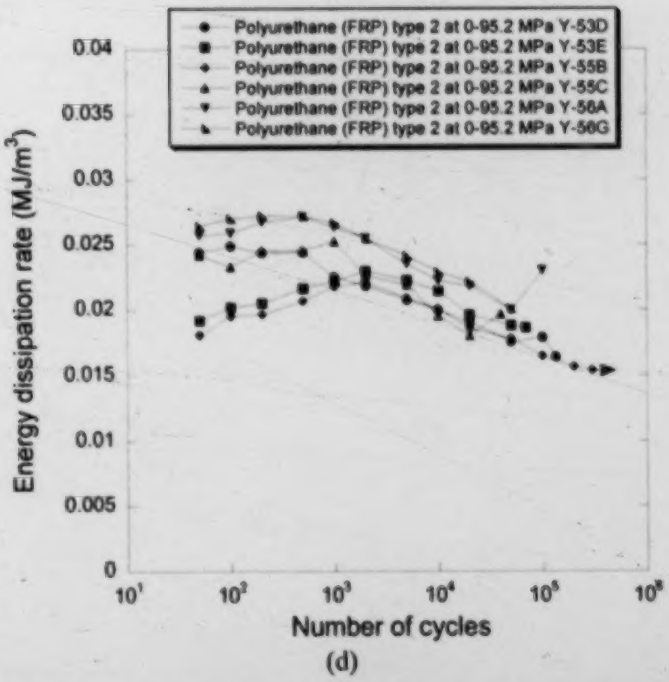

(d)

Figure 4.10. Semi-logarithmic plots of energy dissipation rate versus number of cycles: (a) polyester-based FRP, (b) polyurethane-based FRP type 1, (c) polyurethane-based FRP type 2 at 0-95.2 MPa, and (d) polyurethane-based FRP type 2 at 0-87.6 MPa.

Figure 4.11 depicts typical energy dissipation rates among the FRPs by selecting two specimens from each FRP. Polyurethane-based FRP type 2 at 0-95.2 MPa had the highest energy dissipation rate because the applied stress level was higher than that of the other FRPs. Polyurethane-based FRP type 1 and polyurethane-based FRP type 2 at 0-87.6 MPa had a similar energy dissipation rate, but higher than that of polyester-based FRP because of the same reason. The overall behaviour of energy dissipation rate of polyurethane-based FRP increased slightly in the early cycles up to about approximately 1,000 cycles; while for polyester-based FRP, energy dissipation rate was nearly constant. Afterwards, energy dissipation rate of the polyurethane-based FRP decreased for quite a long time and increased again at the end of fatigue life; while for the polyester-based FRP, it increased from about 1,000 cycles until the end of fatigue life. It was observed that the overall variation of energy dissipation rate in polyurethane-based FRP type 1 and 2 followed the same trend.

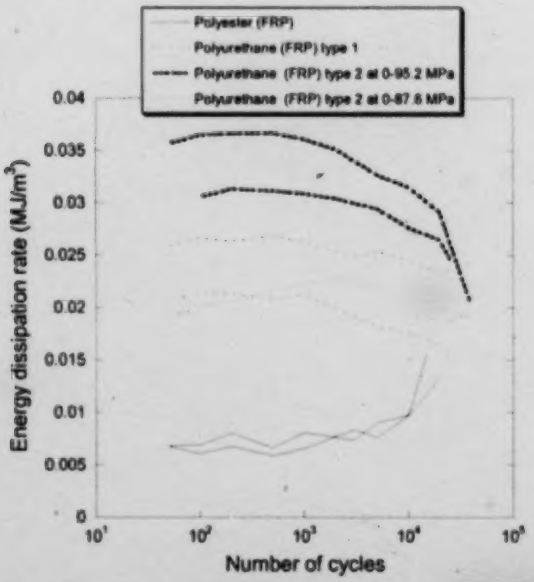

Figure 4.11. A typical semi-logarithmic plot of energy dissipation rate versus number of cycles of FRPs.

4.2.2 Macroscopic and Microscopic Observations

Visual inspection during the test suggested that whitening bands were increasingly generated across the specimen width in the gauge section. Images of specimens before and after the fatigue testing, which were taken using a digital camera, are shown in Figure 4.12. Contrast for the cracks was enhanced using a fluorescent liquid penetrant under black light [56]. Virgin specimens of polyester- and polyurethane-based FRPs (photographs on the left-hand side of Figure 4.12) showed only surface defects around fibers. After fatigue loading (photographs on the right-hand side of Figure 4.12), polyester-based FRP showed extensive cracking through the specimen width, in the direction perpendicular to the loading [13], which is a phenomenon similar to that shown in tensile-fractured specimen (Figure 4.4 (a)) but with a smaller number of cracks. For the polyurethane-based FRP type 1, such a type of cracks cannot be found, but surface defects around the fiber seemed to have grown along the fiber direction. These photographs indicate that the damage development process in the FRPs is progressive in nature, with a distinctive difference between the two FRPs. Comparing polyurethane-based FRP type 1 and polyurethane-based FRP type 2 after fracture, the damage was less intensive in latter. This indicates that voids influence resistance to damage development under fatigue loading for the FRP.

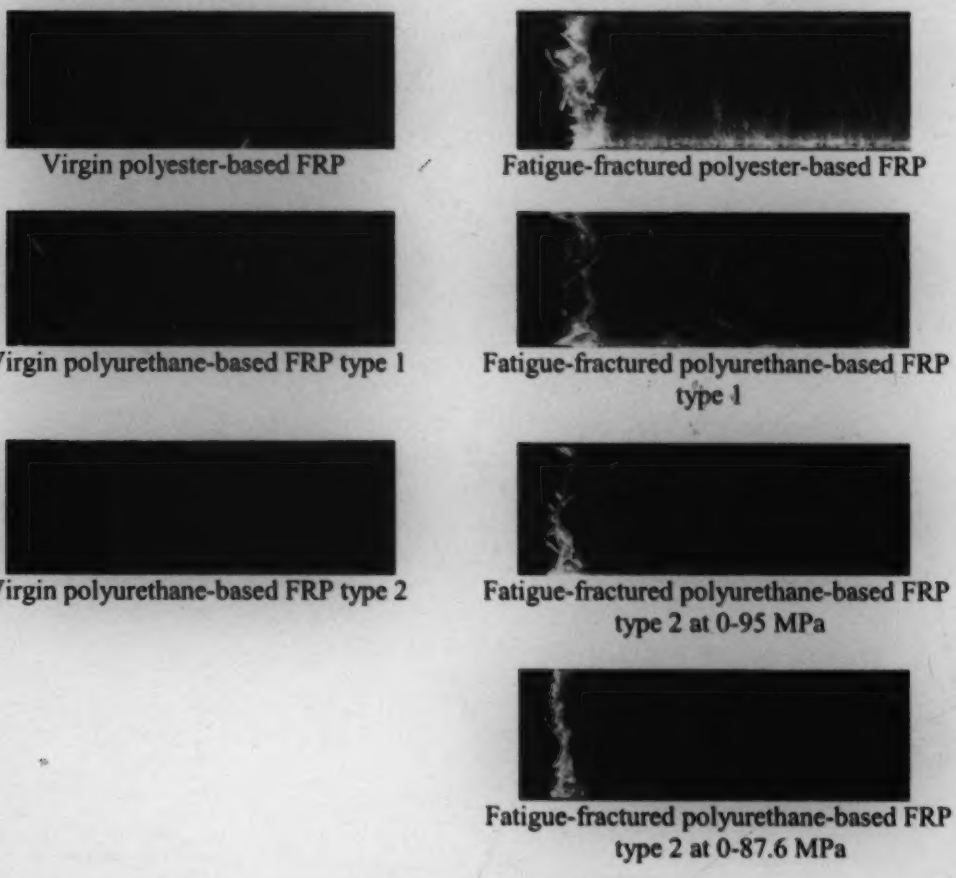
Virgin polyester-based FRP
Fatigue-fractured polyester-based FRP
Virgin polyurethane-based FRP type 1
Fatigue-fractured polyurethane-based FRP type 1
Virgin polyurethane-based FRP type 2
Fatigue-fractured polyurethane-based FRP type 2 at 0-95 MPa
Fatigue-fractured polyurethane-based FRP type 2 at 0-87.6 MPa

Figure 4.12. Photographs of virgin (left-hand side) and fatigue-fractured FRPs (right-hand side).

Figures 4.13, 4.14, 4.15, and 4.16 show the general damage development in the FRPs at different stages of fatigue loading, viewed from the specimen edge (in the Y-direction of Figure 3.2). The Y-direction was chosen because inspection in this direction was found to be more practicable than other directions to detect the cracks. Figure 4.13 (a) was taken from a polyester-based FRP specimen after 1,000 cycles of fatigue loading where extensive cracking was observed but mainly confined within the fiber bundles, as shown by a white arrow. A few matrix cracks were observed, as shown by a black arrow.

Interfacial cracks occurred at first because of poor wetting or defects in FRPs, as reported by several researchers [11,15,16]. When interfacial cracks passed through the width of fiber bundle, the cracks were then grown to the matrix. In the area of random fiber composites, the cracks generated within the fiber bundles are known as "interfacial cracks", due to their formation mainly at the fiber/matrix interface. The cracks in the resin-rich regions, on the other hand, are known as "matrix cracks", due to their occurrence being in the matrix of the specimen. After fatigue fracture, Figure 4.13 (b), extensive matrix cracking was observed in the resin-rich regions. The two micrographs in Figures 4.13 (a) and (b) suggest that the intensive matrix cracks should have been developed sometime after 1,000 cycles from the interfacial cracks. Extensive studies on damage development in polyester-based FRPs were conducted by counting the number of cracks [11] and using nondestructive tests [57,58] but were not attempted here.

The damage development process in the polyurethane-based FRP type 1 is summarized in Figure 4.14. Figure 4.14 (a) was taken from a specimen after 1,000 cycles of fatigue loading. Black, circular regions are voids that, as mentioned before, were caused by trapped air, CO_2 and other vapor phases generated during the curing process. The figure shows many interfacial cracks, as indicated by the white arrow. The cracks favorably grew from interfacial cracks due to slender shape of the cracks that provided higher stress concentration than voids at the crack tip. After 10,000 cycles of fatigue loading, some matrix cracks were about to develop, as indicated by the white arrow in Figure 4.14 (b). The growth of the cracks was found from the crack passing through the interfacial cracks and voids. It was believed that the interfacial cracks were likely to grow

to the nearest voids possibly because of the overlapping of stress concentration generated by the cracks and voids.

(a)

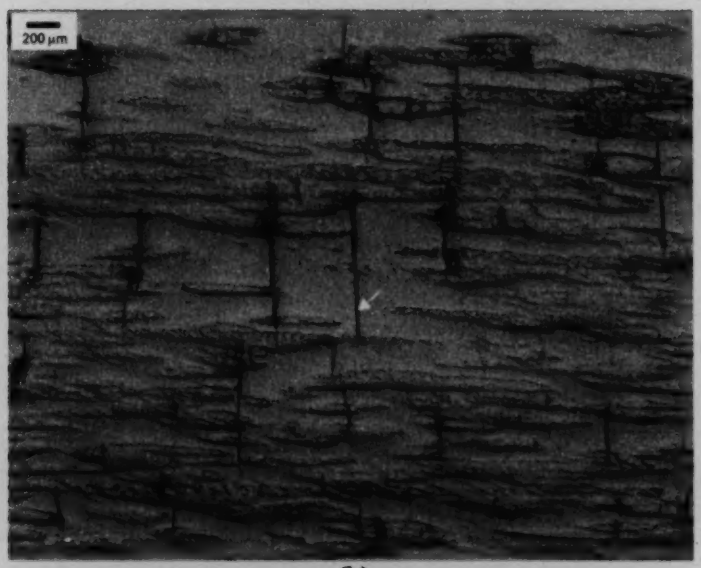

(b)

Figure 4.13. Micrographs viewed in Y-direction (referred to Figure 3.2) of polyester-based FRP: (a) 1,000 cycles, where the matrix cracking was about to develop and (b) 52,897 cycles (fracture).

Voids could function in two different scenarios: assisting the crack propagation or acting as a stress concentrator. A void assisted the crack propagation when the void was located in between two fiber bundles that are adjacent to each other. Interfacial cracks propagated to the void and then to the adjacent fiber bundle. In this scenario, the voids lengthened the crack (black arrows in Figure 4.14 (b)). In the other scenario, a void may be deemed to act as a crack arrester when interfacial cracks grew to the void, or to the matrix and then to void. The changing mode of the sharp crack tip from interfacial cracks (high stress concentration) to blunted crack tip from the voids (low stress concentration) would stop the crack. However, when one end of the crack stopped growing, the other end of the crack would grow further to the matrix (white arrow in Figure 4.14 (b)) and find another "weak area", possibly a void. Thus, the overall role of voids in this scenario is to act as a stress concentrator by increasing the effective crack length.

The fracture could have occurred purely from the first scenario if the voids and fiber bundles had aligned in series, perpendicular to the loading direction. Possible fracture mechanism is that these voids helped to create longer cracks by connecting interfacial cracks from different locations. In this scenario, the matrix toughness could not have a significant role in the fatigue properties of FRP. On the other hand, if the voids only act as a crack arrester, but increasing the overall crack length through matrix, the matrix toughness is important in enhancing fatigue resistance of the FRP. For example, well-developed matrix cracks could be found after 40,000 cycles, but these cracks could not be further developed immediately to initiate specimen fracture, as shown by the white arrow in Figure 4.14 (c).

(a)

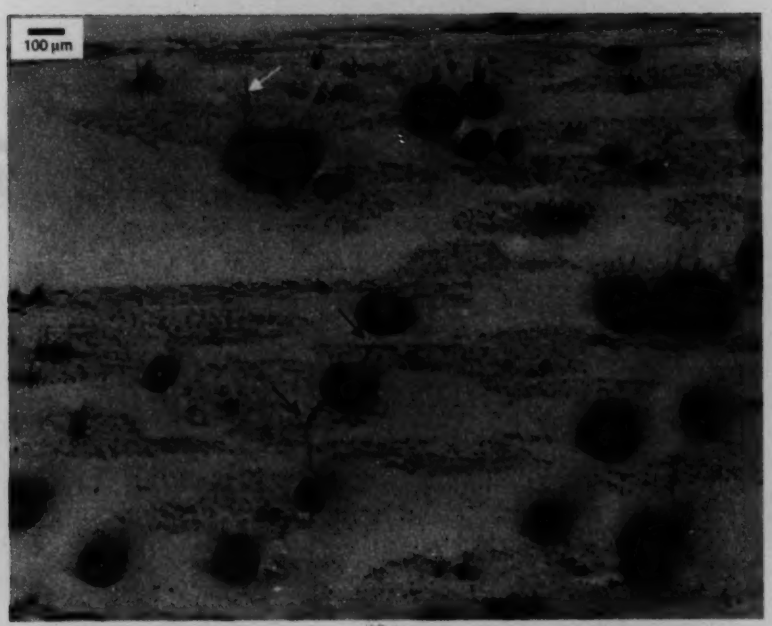

(b)

(continued...)

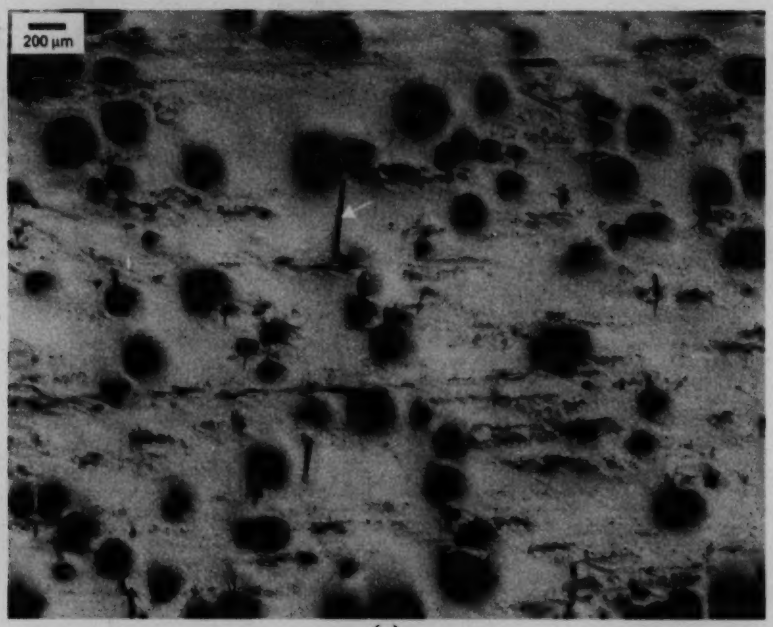

(c)

Figure 4.14. Micrographs viewed in Y-direction (referred to Figure 3.2) of polyurethane-based FRP type 1: (a) 1,000 cycles, where no matrix cracking was developed, (b) 10,000 cycles, where matrix cracking was about to develop, and (c) 40,000 cycles, where matrix cracking had been developed.

The damage development process in the polyurethane-based FRP type 2 at 0-95.2 MPa is summarized in Figure 4.15. Figure 4.15 (a) was taken from a specimen after 1,000 cycles of fatigue loading. Interfacial cracks were observed as shown by the white arrow in the figure. After 10,000 cycles of fatigue loading, some matrix cracks were about to develop from the interfacial cracks, as shown by the white arrow in Figure 4.15 (b). At around 40,000 cycles, matrix cracks were developed from the interfacial cracks and voids that were connected, as shown by the white arrow in Figure 4.15 (c). The damage development of polyurethane-based FRP type 2 at 0-95.2 MPa was found to be similar to that of polyurethane-based FRP type 1.

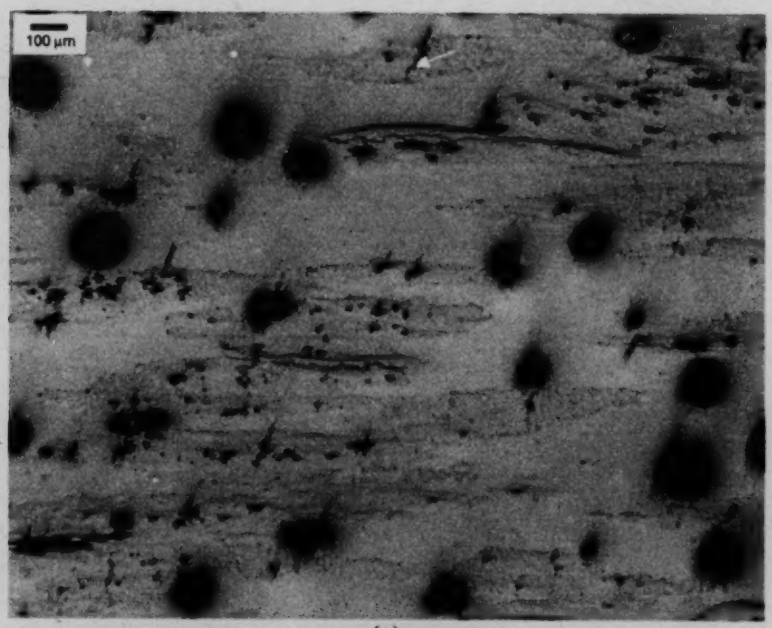

(a)

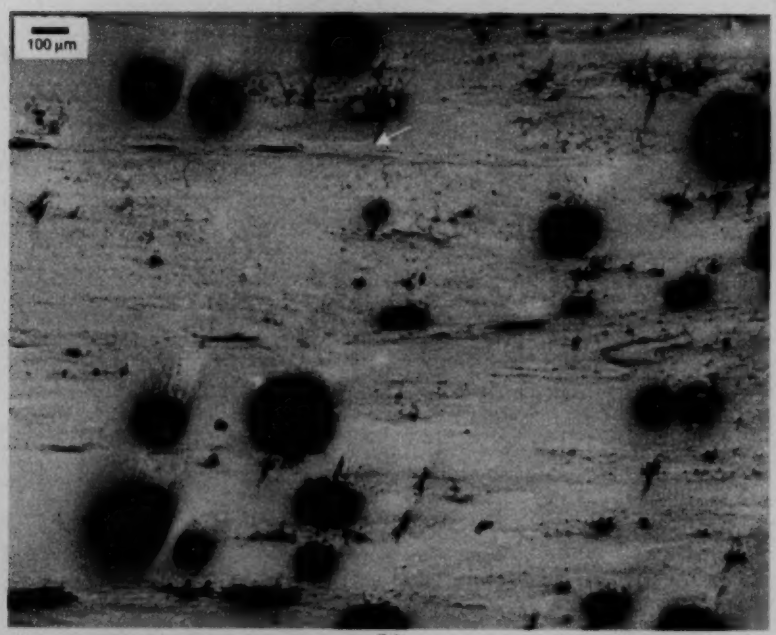

(b)

(continued...)

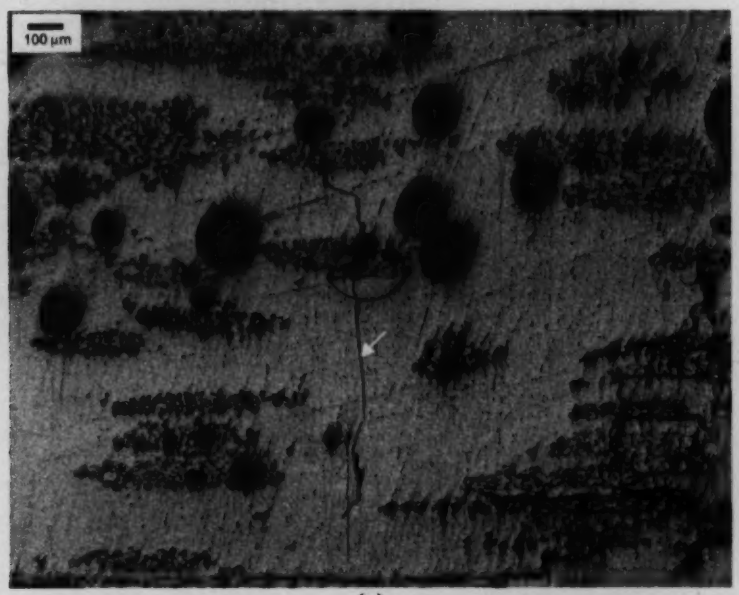

(c)

Figure 4.15. Micrographs viewed in Y-direction (referred to Figure 3.2) of polyurethane-based FRP type 2 at 0-95.2 MPa: (a) 1,000 cycles, where no matrix cracking was developed, (b) 10,000 cycles, where matrix cracking was about to develop, and (c) 39,001 cycles (fracture), where matrix cracking had been developed.

The damage development process in the polyurethane-based FRP type 2 at 0-87.6 MPa is summarized in Figure 4.16. Figure 4.16 (a) was taken from a specimen at 1,000 cycles of fatigue loading. Interfacial cracks were found, as indicated by the white arrow. After 10,000 cycles of fatigue loading, most of the interfacial cracks were still confined in the fiber bundle regions, as indicated by the white arrow in Figure 4.16 (b). Figure 4.16 (c) shows matrix cracking at an early stage of growth from the interfacial cracks at 40,000 cycles, as indicated by white arrow. Figure 4.16 (d) shows the fatigue-fractured specimen in which the well-developed matrix cracks could be found but the number is small. The crack shown in the figure was passing through interfacial cracks and void. The micrographs suggest that the lower void content has delayed matrix cracking from 10,000

cycles (in polyurethane-based FRP type 1) to 40,000 cycles (in polyurethane-based FRP type 2) at the same stress level because number of voids available to assist matrix crack growth was reduced. In other words, the interfacial cracks were "reluctant" to grow to the matrix because of fewer voids, meaning that the matrix has "less weak area".

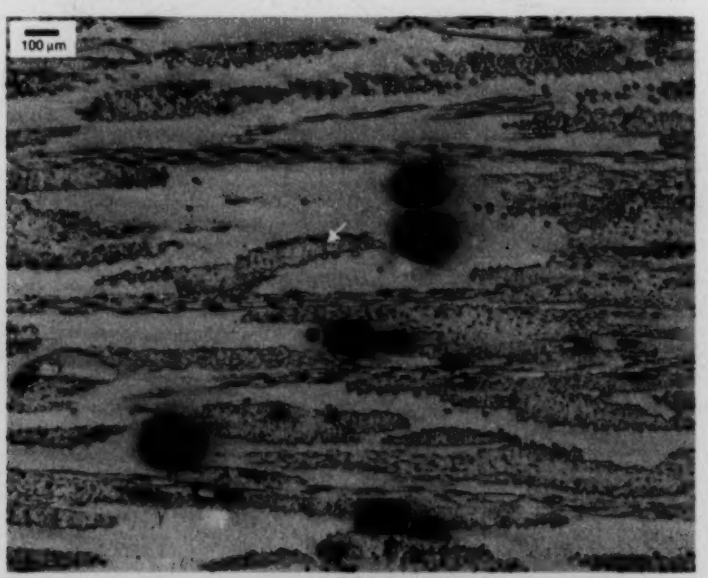

(a)

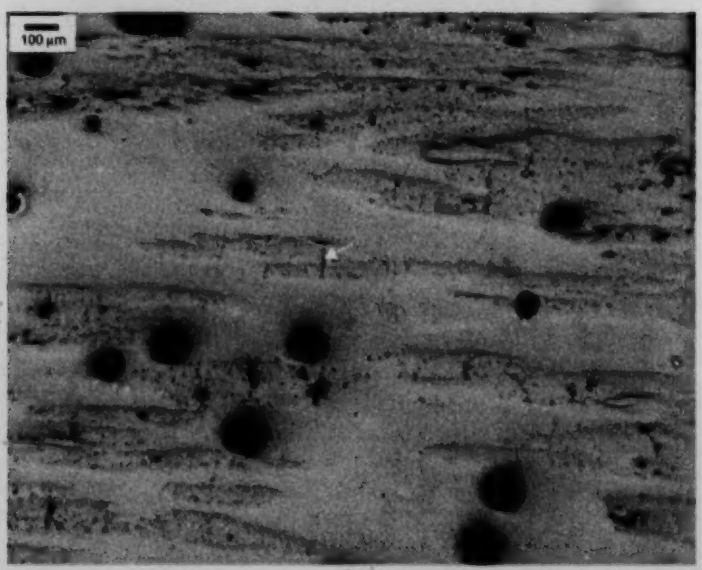

(b)

(continued...)

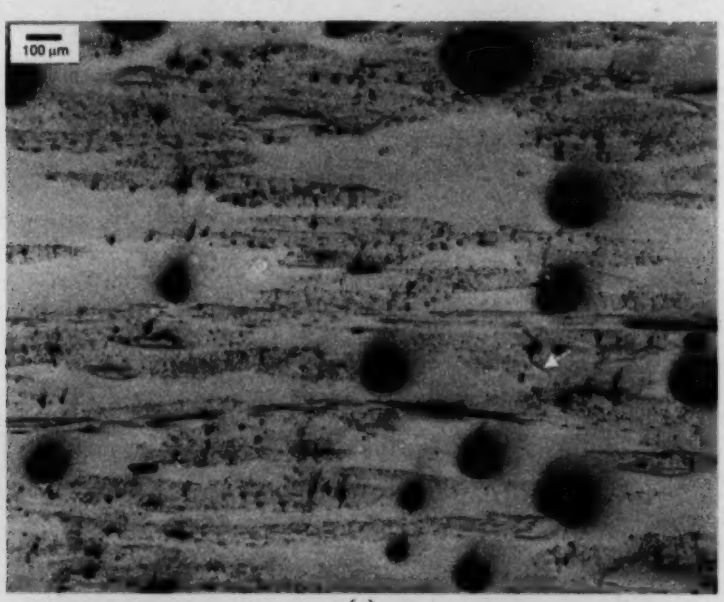

(c)

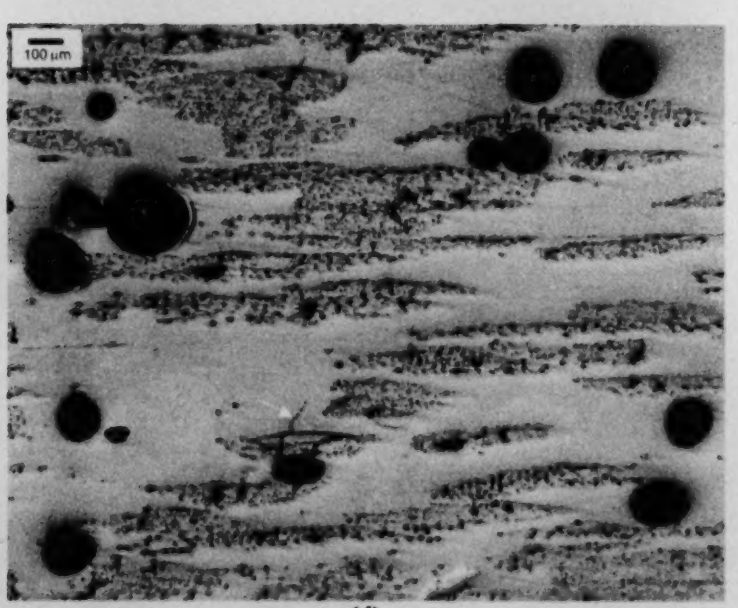

(d)

Figure 4.16. Micrographs viewed in Y-direction (referred to Figure 3.2) of polyurethane-based FRP type 2 at 0-87.6 MPa: (a) 1,000 cycles, where few interfacial cracks were observed, (b) 10,000 cycles, where many interfacial cracks were observed, (c) 40,000 cycles, where matrix cracking was about to develop, and (d) 69,882 cycles (fracture), where matrix cracking had been developed.

Comparison of the micrographs in Figures 4.13 for polyester-based FRP and 4.14 for polyurethane-based FRP type 1 revealed the difference in the damage development process between the two FRPs. Both FRPs showed the development of interfacial cracks within the first 1,000 cycles of fatigue loading. However, in contrast to the polyester-based FRP that developed matrix cracking soon afterwards, the polyurethane-based FRP type 1 had the interfacial cracks stabilized for quite a long time before the matrix cracks were eventually developed from the interfacial cracks to voids to form longer cracks. This was similar to that observed in polyurethane-based FRP type 2 at 0-95.2 MPa which was shown in the Figure 4.15. The delay of matrix cracking in the polyurethane-based FRP rendered a longer fatigue lifetime than that of polyester-based counterpart. When cycled at the same absolute stress level as polyurethane-based FRP type 1, the polyurethane-based FRP type 2 had better fatigue resistance by delaying matrix cracking to a higher number of cycles, due to its lower void content, and thus increasing the fatigue lifetime. The above observation has been confirmed by several examinations of the FRPs at different stages of the fatigue loading.

4.3 Plain-strain Fracture Toughness Tests

Fracture toughness measures a material's resistance to brittle fracture when a crack is present. Fracture toughness tests were conducted on pure resin casts. The results are shown in Tables 4.10 for polyester and 4.11 for polyurethane. Crack length, a, was averaged from 3 positions: at the center of the crack front and the two ends of the crack front, according to the standard. Since the value of σ_y used for polyester is conservative

(due to occurrence of tensile fracture in the neck of the specimens), the value in the right column in Table 4.10, $2.5(k_Q/\sigma_y)^2$, must be larger than the true values, should true σ_y have been used for the calculation. Therefore, there is no doubt that the condition given by Equation (3.2), $B,a,(W-a) > 2.5(K_Q/\sigma_y)^2$, is satisfied. Hence, K_Q is valid to be called K_{IC} of the polymers. It was found that the fracture toughness of polyurethane was slightly over 4 times of that of polyester. This is believed to be the main reason for the polyurethane-based FRP to be more resistant to matrix crack propagation than polyester-based FRP.

Table 4.10. K_{IC} of polyester.

Specimen name	a (mm)	$f(x)$	P_Q (kN)	K_Q (MPa m$^{1/2}$)	σ_y (MPa)	$2.5(k_Q/\sigma_y)^2$ (mm)
E-14	5.9	10.37	0.023	0.37	47	0.154
E-15	6.2	11.24	0.019	0.33	47	0.123
E-19	5.8	10.11	0.027	0.41	47	0.192
E-20	6.1	10.94	0.022	0.36	47	0.15
Mean				**0.37**		
Standard deviation				**0.03**		

Table 4.11. K_{IC} of polyurethane.

Specimen name	a (mm)	$f(x)$	P_Q (kN)	K_Q (MPa m$^{1/2}$)	σ_y (MPa)	$2.5(k_Q/\sigma_y)^2$ (mm)
U-14	6.1	10.94	0.079	1.32	80.2	0.673
U-19	6.3	11.55	0.091	1.60	80.2	0.989
U-21	5.6	9.61	0.107	1.56	80.2	0.943
U-22	5.4	9.14	0.124	1.72	80.2	1.147
Mean				**1.55**		
Standard deviation				**0.17**		

The fracture toughness, K_{IC}, of the polymer, which was measured under static loading, was reported to be transferable to the fatigue loading, for evaluating its critical

stress intensity factor, K_C [59]. The study showed that under fatigue loading, K_C is associated with K_{IC} of the material, provided that the plastic flow is confined to the crack tip. Since the fiber reinforcement and distribution were similar among the FRPs used in the study, it is reasonable to assume that confinement of plastic flow is the same among the FRP used in this study. Therefore, the high K_{IC} for polyurethane has generated a significant resistance to crack growth in the matrix of its FRP, compared to that of the polyester-based counterpart.

4.4 Synthesis of the Fatigue Behaviour

By combining the mechanical testing of linear plot of modulus degradation shown in Figure 4.9 (b) and the images in Figures 4.13, 4.14, 4.15, and 4.16 for polyester-based FRP, polyurethane-based FRP type 1, polyurethane-based FRP type 2 at 0-95.2 MPa, and polyurethane-based FRP type 2 at 0-87.6 MPa, the following damage development process is suggested. During the first 1,000 cycles of fatigue loading, interfacial cracks were initiated in the fiber bundles for both FRPs, causing a sharp drop of the modulus. The interfacial cracks in the polyester-based FRP quickly led to the development of matrix cracks, due to low toughness of polyester, causing further drop of the modulus and eventually leading to the specimen fracture.

For the polyurethane-based FRP, on the other hand, the matrix was tough enough to resist the development of matrix cracking from the interfacial cracks. Therefore, modulus of polyurethane-based FRP showed little change after around 1,000 cycles. When matrix cracking from the interfacial cracks has grown in the polyurethane-based

FRP with the assistance from voids in the matrix, the modulus dropped further that led to the specimen fracture. By reducing the number of voids, the fatigue lifetime of polyurethane-based FRP, such as type 2 at 0-87.6 MPa, was increased. The slight decrease of fatigue lifetime for polyurethane-based FRP type 2 at 0-95.2 MPa was probably due to a higher applied stress level. However, the damage development in polyurethane-based FRP type 1 and polyurethane-based FRP type 2 at 0-95.2 MPa were found to be similar. It was noticed that the modulus for polyurethane-based FRP only dropped at the end of the fatigue life, probably due to the growth of matrix cracks that led to final fracture.

By applying the above understanding of the damage development process to the energy dissipation rate shown in Figure 4.11, it is believed that the high level of energy dissipation rate for the polyurethane-based FRP in the first 1,000 cycles is an indication of a relatively strong bonding between polyurethane and glass fiber shown by a smaller number of interfacial cracks, as compared to polyester-based FRP. The strong bonding resulted in the increase of energy dissipation for generation of interfacial crack. The increase of energy dissipation rate of polyester-based FRP that occurred after 1,000 cycles was probably due to the development of matrix cracking, to allow fiber pull-out and/or fiber re-orientation during the fracture process. For polyurethane-based FRP type 1, the interfacial cracks were saturated sometime after 1,000 cycles, but did not lead to extensive matrix cracking. Therefore, its energy dissipation rate dropped slightly after 1,000 cycles. When the matrix cracking was eventually initiated from interfacial cracks to voids, its energy dissipation rate increased again, as evident in some curves, but its occurrence was very close to the final fracture of the specimen.

Polyurethane-based FRP type 2 at 0-95.2 MPa showed the same behaviour as that of polyurethane-based FRP type 1, but had a higher energy dissipation rate due to a higher level of applied stress. For polyurethane-based FRP type 2 at 0-87.6 MPa, energy dissipation rate showed the same trend as that of the polyurethane-based FRP type 1, but its fatigue lifetime was increased. This was probably due to less matrix damage generated from interfacial cracks because of fewer occurrences of voids.

5. Conclusions and Recommendations for the Future Studies

This study examined mechanical properties of polymers under tensile loading and their FRPs under tensile and fatigue loading. It was found that under tensile loading there was definitely a correlation of properties between resin casts and the corresponding FRPs. Polyurethane and polyurethane-based FRP showed higher ultimate tensile strength and strain to failure, compared to those of polyester and polyester-based FRP. Microscopic observations of the fractured FRP specimens showed a significant difference in the crack appearance.

Fatigue tests were conducted on FRPs at the zero-tension mode, with the maximum stress equivalent to 50% of their respective UTS. Polyester-based FRP showed inferior fatigue lifetime, compared to that of polyurethane-based FRP. Variations in modulus and energy dissipation rate of the FRPs were correlated with the damage development process. The rise of energy dissipation rate for the polyurethane-based FRP at the early cycles was due to its strong bonding between fiber and matrix that incurred noticeable energy loss for crack formation at the interface. However, the high bonding strength was not sufficient to prevent the development of interfacial cracks in the polyurethane-based FRP. It was found that better fatigue resistance of the polyurethane-based FRP mainly came from the tougher polyurethane matrix that resisted the development of matrix cracks.

Polyester-based FRP showed the damage development from interfacial cracks to matrix cracking in a relatively continuous manner; while polyurethane-based FRP in a

discontinuous manner, that is, the tough matrix has slowed down the development of matrix cracking from the interfacial cracks. The damage development process in the polyurethane-based FRP was believed to be from the interfacial cracks to voids, or to the matrix and then to voids, which later coalesced to form the fracture surface. Voids played two roles in the fracture formation process. One was to assist the crack propagation by increasing the crack length and the other to act as a crack arrester. However, the overall role of the voids was to enhance the stress concentration, thus assisting the development of matrix cracking, and reducing the fatigue lifetime. Decrease of the void content in the polyurethane-based FRP type 2, when subject to the same absolute fatigue stress level as that of polyurethane-based FRP type 1, showed increase in the fatigue lifetime. This was believed to be due to fewer voids that delayed the matrix cracking.

From the study conducted above, the following recommendations are proposed to continue the study.

1) For ideal cases of comparison, void-free polyurethane-based FRP is desired, as decrease of void content is expected to increase the fatigue lifetime. In such cases, fracture is expected to generate from interfacial cracks to matrix cracking. However, the number of cracks is expected to be lower than that of polyester-based FRP due to tough polyurethane matrix.

2) It will be interesting to extend the study to cover the whole fatigue damage processes by varying the stress level and examining the corresponding change in modulus degradation and energy dissipation rate under fatigue loading. The damage development is expected to change by varying the stress level. However,

the tough polyurethane matrix is still expected to enhance fatigue resistance of its FRP.

3) Further investigation of the onset of interfacial cracks and matrix cracking can be of great interest and complementary to current study. In-situ study of crack propagation should be conducted from the beginning to the end of the fatigue lifetime. Quantifying the number of cracks in polyester- and polyurethane-based FRP may provide some insight information that cannot be revealed from the current study. This proposed study may provide useful information to prove the damage development model presented in this thesis.

4) Study of the effects of specimen geometry may be worthwhile. Wider specimen size will be beneficial for increasing the effective fiber length for reinforcement. Therefore, better mechanical properties and fatigue performance are expected.

6. Bibliography

[1] L. J. Broutman, "Modern Composite Materials", pp. 3-8, Addison-Wesley Publishing Company, Massachusetts (1967).

[2] B. Parkyn, "Glass Reinforced Plastics", pp. 3-7, Butterworth & Co Ltd., Norwich (1970).

[3] R. W. Hertzberg and J. A. Manson, "Fatigue of Engineering Plastics", pp. 184-277, Academic Press, New York (1980).

[4] B. Harris, "Fatigue and Accumulation of Damage in Reinforced Plastics", Composites, Vol. 8, pp. 214-220 (1977).

[5] D. Dew-Hughes and J. L. Way, "Fatigue Fibre-reinforced Plastics: A Review", Composites, Vol. 4, pp.167-173 (1973).

[6] P. T. Curtis and G. Dorey, "Fatigue of Composite Materials", Fatigue of Engineering Materials and Structures, Vol. 2, pp. 297-306 (1986).

[7] R. Talreja, "Fatigue of Composite Materials: Damage Mechanisms and Fatigue-life Diagrams", Proceedings of the Royal Society of London, Vol. A378, pp. 461-475 (1981).

[8] M. Van Der Oever and T. Peijs, "Continuous-glass-fibre-reinforced Polypropylene Composites: II. Influence of Maleic-anhydride Modified Polypropylene on Fatigue Behaviour", Composites Part A, Vol. 29, pp. 227-239 (1998).

[9] S. L. Kim, M. D. Skibo, J. A. Monson, R. W. Hertzberg, and J. Janiszewski, "Tensile, Impact, and Fatigue Behaviour of an Amine-cured Epoxy Resin", Polymer Engineering and Science, Vol. 18, pp. 1093-1100 (1978).

[10] T. R. Smith and M. J. Owen, "Fatigue Properties of RP", Modern Plastics, Vol. 46, pp. 124-132 (1969).

[11] M. J. Owen and M. J. Howe, "The Accumulation of Damage in a Glass-reinforced Plastic under Tensile and Fatigue Loading", Journal of Physics D: Applied Physics, Vol. 5, pp. 1637-1649 (1972).

[12] R. Talreja, "Fatigue of Composite Materials", pp. 73-81, Technomic Publishing Company, Pennsylvania. (1987).

[13] S. S. Wang and E. S. -M. Chim, "Fatigue Damage and Degradation in Random Short-fiber SMC Composite", Journal of Composite Materials, Vol. 17, pp.114-134 (1983).

[14] T. R. Smith and M. J. Owen, "Progressive Nature of Fatigue Damage in RP", Modern Plastics, Vol. 46, pp.128-133 (1969).

[15] M. J. Owen, T. R. Smith, and R. Dukes, "Failure of Glass-reinforced Plastics, with Special Reference to Fatigue", Plastics and Polymers, Vol. 37, pp. 227-233 (1969).

[16] M. J. Owen and R. G. Rose, "Polyester Flexibility versus Fatigue Behaviour of RP", Modern Plastics, Vol. 47, pp. 130-138 (1970).

[17] T. K. O'Brien and K. L. Reifsnider, "Fatigue Damage: Stiffness/Strength Comparisons for Composite Materials", Journal of Materials Testing and Evaluation, Vol. 5 pp. 384-393 (1977).

[18] H. C. Kim and L. J. Ebert, "Axial Fatigue Failure Sequence and Mechanisms in Unidirectional Fiberglas Composites", Journal of Composite Materials, Vol. 12, pp. 139-152 (1978).

[19] K. Hellan, "Introduction to Fracture Mechanics", pp. 49-69, McGraw-Hill Book Company, New York (1984).

[20] H. A. Aglan, Y. X. Gan, F. Chu, and W. H. Zhong, "Fatigue Fracture Resistance Analysis of Polymer Composites Based on the Energy Expended on Damage Formation", Journal of Reinforced Plastics and Composites, Vol. 22, pp. 339-360 (2003).

[21] F. Ellyin, "Fatigue Damage, Crack Growth, and Life Prediction", pp. 86-89, Chapman and Hall, London (1997).

[22] A. C. Soldatos, A. S. Burhans, and C. F. Cole, "Correlation Between High Performance Epoxy and Cast Resin Properties and Composite Performance", 24th SPI Reinforced Technical Conference, pp. 1-6 (1969).

[23] E. K. Gamstedt and R. Talreja, "Fatigue Damage Mechanisms in Unidirectional Carbon-fibre-reinforced Plastics", Journal of Materials Science, Vol. 34, pp. 2535-2546 (1999).

[24] R. J. Sanford and F. R. Stonesifier, "Fracture Toughness Measurements in Unidirectional Glass-reinforced-plastics", Journal of Composite Materials, Vol. 5, pp. 241-245 (1971).

[25] M. E. Waddoups, J. R. Eisenmann, and B. E. Kaminski, "Macroscopic Fracture Mechanics of Advanced Composite Materials", Journal of Composite Materials, Vol. 5, pp. 446-454 (1971).

[26] M. J. Owen and P. T. Bishop, "The Significant of Microdamage in Glass-reinforced Plastics at Macroscopic Stress Concentrators", Journal of Physics D: Applied Physics, Vol. 5, pp. 1621-1636 (1972).

[27] H. J. Konish, J. L. Swedlow, and T. A. Cruse, "Experimental Investigation of Fracture in an Advanced Fiber Composite", Journal of Composite Materials, Vol. 6, pp. 114-124 (1972).

[28] M. J. Owen and P. T. Bishop, "Fatigue Properties of Glass-reinforced Plastics Containing a Stress Concentrator", Journal of Physics D: Applied Physics, Vol. 6, pp. 2057-2069 (1973).

[29] M. J. Owen and P. T. Bishop, "Critical Stress Intensity Factors Applied to Glass Reinforced Polyester Resin", Journal of Composite Materials, Vol. 7, pp. 146-159 (1973).

[30] J. F. Mandell, S. S. Wang, and F. J. McGarry, "The Extension of Crack Tip Damage Zones in Fiber Reinforced Plastics Laminates", Journal of Composite Materials, Vol. 9, pp. 266-287 (1975).

[31] S. Gaggar and L. J. Broutman, "Crack Growth Resistant of Random Fiber Composites", Journal of Composite Materials, Vol. 9, pp. 216-227 (1975).

[32] S. K. Gaggar and L. J. Broutman, "Effect of Crack Tip Damage on Fracture of Random Fiber Composites", Materials Science and Engineering, Vol. 21, pp. 177-183 (1975).

[33] F. J. McGarry, J. F. Mandell, and S. S. Wang, "Fracture Fiber Reinforced Composites", Polymer Engineering and Science, Vol. 16, pp. 609-614 (1976).

[34] S. K. Gaggar and L. J. Broutman, "Strength and Fracture Properties of Random Fibre Polyester Composites", Fibre Science and Technology, Vol. 9, pp. 205-224 (1976).

[35] J. F. Mandell, A. Y. Darwish, and F. J. McGarry, "Fracture Testing of Injection-molded Glass and Carbon Fiber-reinforced Thermoplastics", ASTM STP 734, pp. 73-90 (1981).

[36] B. D. Agarwal and G. S. Giare, "Influence of the Properties of the Matrix Material on the Fracture Toughness of Short-fibre Composites", Materials Science and Engineering, Vol. 52, pp. 139-145 (1982).

[37] S. S. Wang, E. S. -M. Chim, T. P. Yu, and D. P. Goetz, "Fracture of Random Short-fiber SMC Composite", Journal of Composite Materials, Vol. 17, pp. 299-315 (1983).

[38] J. F. Mandell, F. J. McGarry, and C. G. Li, "Fatigue Crack Growth and Lifetime Trends in Injection Molded Reinforced Thermoplatics", ASTM STP 873, pp. 36-50 (1985).

[39] J. F. Mandel, "Fatigue of Composite Material", Vol. 4, pp. 231-337, Elsevier, New York (1991).

[40] M. J. Owen and P. T. Bishop, "Crack-growth Relationships for Glass-reinforced Plastics and Their Application to Design", Journal of Physics D: Applied Physics, Vol. 7, pp. 1214-1224 (1974).

[41] J. F. Mandell, "Fatigue Crack Propagation Rates in Woven and Nonlinear Fiber Glass Laminates", ASTM STP 580, pp. 515-546 (1975).

[42] S. S. Wang, E. S. -M. Chim, and N. M. Zahlan, "Fatigue Crack Propagation in Random Shot-fiber SMC Composite", Journal of Composite Materials, Vol. 17, pp. 250-266 (1983).

[43] G. A. Cooper and A. Kelly, "Tensile Properties of Fibre-reinforced Metals: Fracture Mechanics", Journal of the Mechanics and Physics of Solids, Vol. 15, pp. 279-297 (1967).

[44] C. Zweben, "On the Strength of Notched Composites", Journal of the Mechanics and Physics of Solids, Vol. 19, pp. 103-116 (1971).

[45] M. Biron, "Thermosets and Composites", pp. 32-144, Elsevier Advanced Technology, Oxford (2004).

[46] A. K. Kaw, "Mechanics of Composite Materials", pp. 2-50, CRC Press, Florida (1997).

[47] J. R. Lawrence, "Polyester Resins", pp. 1-12, Reinhold Publishing Corporation, New York (1960).

[48] K. A. Olivero, H. J. Barraza, E. A. O'Rear, and M. C. Altan, "Effect of Injection Rate and Post-fill Cure Pressure on Properties of Resin Transfer Molded Disks", Journal of Composite materials, Vol. 36, pp. 2011-2028 (2002).

[49] N. Pearce, F. Guild, and J. Summerscales, "A Study of the Effects of Convergent Flow Fronts on the Properties of Fibre Reinforced Composites Produced by RTM", Composite Part A, Vol. 29A, 141-152 (1998).

[50] American Society for Testing and Materials (ASTM) Standard D 3171-99: Standard Method for Constituent Content of Composite materials, Vol. 15.03 (2003).

[51] American Society for Testing and Materials (ASTM) Standard D 638-01: Standard Test Method for Tensile Properties of Plastics, Vol. 08.01 (2002).

[52] J. W. Dally and L. J. Broutman, "Frequency Effects on the Fatigue of Glass-reinforced Plastics", Journal of Composite Materials, Vol. 1, pp. 424-442 (1967).

[53] W. Hwang and K. S. Han, "Fatigue of Composites - Fatigue Modulus Concept and Life Prediction", Journal of Composite Materials, Vol. 20, pp. 154-165 (1986).

[54] American Society for Testing and Materials (ASTM) Standard D 5045-99: Standard Method for Plane-Strain Fracture Toughness and Strain Energy Release Rate of Plastic Materials, Vol. 8.03 (2003).

[55] J. F. Mandell, D. D. Huang, and F. J. McGarry, "Fatigue Glass and Carbon Fiber Reinforced Engineering Thermoplastics", Polymer Composites, Vol. 2, pp. 137-144 (1981).

[56] American Society for Testing and Materials (ASTM) Standard E 1209-99: Standard Test for Fluorescent Liquid Penetrant Examination Using the Water-Washable Process, Vol. 03.03 (2003).

[57] B. Harris, "Fatigue and Accumulation of Damage in Reinforced Plastics", Composites, Vol. 8, pp. 214-220 (1977).

[58] Ph. Margueres, F. Meraghni, and M. L. Benzeggagh, "Comparison of Stiffness Measurements and Damage Investigation Techniques for a Fatigued and Post-impact Fatigued GFRP Composite Obtained by RTM Process", Composite Part A, Vol. 31, pp. 151-163 (2000).

[59] S. A. Meguid, "Engineering Fracture Mechanics", pp. 243-286, Elsevier Science Publisher, New York (1989).